EQUILIBRIUM AND KINETIC ANALYSIS OF FLUORIDE ADSORPTION ON BONE CHARCOAL

by

JOHN ANDREW JONES

Bachelor of Science in Engineering, Specializing in BME, Mercer University, May 2012

A Thesis Submitted to the Graduate Faculty

of Mercer University School of Engineering

in Partial Fulfillment of the

Requirements for the Degree

MASTER OF SCIENCE IN ENGINEERING

MACON, GA

2012

EQUILIBRIUM AND KINETIC ANALYSIS OF FLUORIDE

ADSORPTION ON BONE CHARCOAL

by

JOHN ANDREW JONES

Approved:

_____ Date _____
Dr. Laura Lackey, Advisor

_____ Date _____
Dr. Edward O'Brien, Committee Member

_____ Date _____
Dr. Caryn Seney, Committee Member

_____ Date _____
Dr. Wade H. Shaw, Dean, School of Engineering

ACKNOWLEDGEMENTS

This work would not have been possible without the confidence that my family, friends, roommates, fellow students, coaches, and educators have shown in me. I thank all of you for putting up with my frustration, procrastination, and the occasional lapse in sanity over the past year that have made this work a success. I would like to dedicate this work to my mom, Andrea Jones. Without her unfaltering confidence in my abilities and clarity in judgement, I would not be who I am today. Mom, never forget that you are M.P.F.

TABLE OF CONTENTS

LIST OF TABLES

LIST OF FIGURES

LIST OF EQUATIONS

ABSTRACT

JOHN ANDREW JONES
EQUILIBRIUM AND KINETIC ANALYSIS OF FLUORIDE ADSORPTION ON BONE CHARCOAL
Under the direction of DR. LAURA LACKEY

The equilibrium capacity and kinetics of fluoride adsorption on to bone charcoal were studied in a batch differential volume reactor. The isotherm models of the Freundlich (R^2 = 0.93) and Halsey (R^2 = 0.93) equations were found to best describe the equilibrium adsorption of fluoride on bone char (BC), while the Elovich model was shown to provide the best description of the time-variant adsorption kinetics. The adsorption capacity of the bone char was found to be slightly favorable with increases in the initial aqueous fluoride concentration leading to higher adsorption capacities. The addition of contact precipitant (CP) pellets to the bone char adsorption system in a 3 to 1 (CP to BC) mass ratio was shown to increase the equilibrium fluoride removal capacity of the system by a factor of approximately three, without altering the adsorption kinetics. The kinetics of removal were compared for a variety of trials including various masses of bone char, ratios of CP pellets, and initial fluoride concentrations. The kinetics were found to remain constant such that after a given contact time, the same percentage of total possible removal for the given configuration would have been achieved. An average best fit

line was developed to describe the adsorption kinetics such that:

$$\% \text{ of Total Capacity} = 17.86 \ln(\text{time}) + 28.53.$$

These findings allow for the fluoride adsorption systems to be designed with emphasis on maximizing the equilibrium adsorption capacity of the system without primary focus on the kinetics of removal.

CHAPTER 1

INTRODUCTION AND BACKGROUND

Fluoride is one of a few elements that exist in the human body for which a delicate balance is held between it as a beneficial additive and a toxic contaminant. At aqueous concentrations up to 1.0 part-per-million (ppm), fluoride has been shown to increase the strength of tooth enamel and decrease the frequency of tooth decay in humans [1–3]. Fluoride concentrations in drinking water greater than 1.5 ppm have been deemed as dangerous to human health by the World Health Organization (WHO) due to a plethora of health effects ranging from unsightly dental fluorosis to crippling skeletal fluorosis [1]. Fluorosis, or the over exposure to fluoride, is conservatively estimated to affect tens of millions worldwide [1]. The most common source of human fluoride ingestion is from drinking water [1]. The high reactivity of fluorine in its natural gaseous state results in low gaseous concentrations. Thus, the ingestion of neutral fluoride gas presents a negligible path of natural contamination for humans [2]. Due to the inert and non-reactive nature of fluoroapatite complexes, bioaccumulation of fluoride is low and therefore fluoride ingestion from food is rare but several varieties of tea have shown elevated fluoride levels [2], [4].

Trace amounts of fluoride can be found in nearly all natural waters around the world and fluoride accounts for approximately 0.06-0.09 mass percent of the earth's crust which results in an average soil concentration of 300mg/kg [1]. This concentration is highly variable depending on the geologic nature of the specific region. Elevated fluoride concentrations can result from contamination due to industrial and manufacturing processes or from many natural sources of fluoride. Fluoride and fluoride containing compounds are commonly found in a variety of minerals including fluorspar, rock phosphate, cryolite, apatite, mica, and hornblende [2]. Regions where these minerals are commonly found also have increased fluoride concentration in the groundwater due to frequent contact and subsequent leaching of fluoride from the bedrock.

Regions of the world with high volcanic activity commonly contain increased levels of fluoride in the soil due to emissions of hydrofluoric acid during eruptions [2]. High fluoride levels can be seen in southwestern North America, Iraq, China, Syria, India, and the Rift Valley in Africa [3]. The Rift Valley transects through a group of countries from Eritrea to Tanzania [2]. Fluoride concentrations of up to 2800 ppm have been reported in the Rift Valley although the average concentration is considerably less [1]. This collection of five countries has some of the highest natural groundwater fluoride concentrations found on earth and much of the current remediation technologies and treatments are focused for this area [2].

The purpose of this work is to better describe the phenomenon of fluoride adsorption on bone char. This phenomenon will be studied from an equilibrium and kinetics perspective. The gained understanding will then be applied to the design of adsorption systems so that a most efficient configuration can be achieved. This work will increase the feasibility and sustainability of the fluoride adsorption systems used in many rural areas and will in turn increase the quality of life for the people who live there.

Removal Strategies

Many strategies have been developed to remove excess fluoride from drinking water. These processes include: Ion Exchange, Membrane separation, Flocculation, and Adsorption processes. Many of the most contaminated regions of the world such as in India and The Rift Valley have a large portion of their population that live in severe poverty and thus the high costs of many remediation technologies present a feasibility concern for those regions. Due to financial constraints, membrane separation processes such as reverse osmosis and ion exchange resins are not available to many of the effected people worldwide.

Nalgonda Technique

The primary flocculation/coagulation technology used for the removal of fluoride is the application of alum ($Al_2(SO_4)_3$) and lime ($Ca(OH)_2$) in a process called the Nalgonda technique. The Nalgonda technique is a primarily batch process where the fluoride contaminated influent is mixed with alum and lime to promote coagulation

and sedimentation of aluminum hydroxide. The aluminum hydroxide flocks electrostatically bind to the dissolved fluoride to pull it out of solution [1]. The batch of water is then filtered within two hours to collect the precipitants before the electrostatic attraction is lost and the fluoride re-enters the defluoridated water [5], [6]. The process is moderately effective with typical removal efficiencies of 70-80% but is incapable of reducing the effluent fluoride concentration below the WHO limit (1.5ppm F^-) for elevated influent concentrations [1], [5], [6]. The Nalgonda technique has many disadvantages including high difficulty of use and elevated levels of sulfate and residual aluminum in the effluent [5]. The Nalgonda technique has been used at the household and community levels for many years but is now being displaced by adsorption technologies due to their simplicity of use.

Adsorption

Adsorption technologies are the primary and preferred method of fluoride removal from drinking water for impoverished people worldwide [1], [7–9]. Many adsorbents have been found to be effective at removing fluoride from aqueous solutions including: fired clay, activated alumina, and bone charcoal. In rural and impoverished areas, the availability of the adsorbent material is a primary concern and thus bone charcoal, derived largely from cow bone, is primarily used. Although cow bone is the primary source, sheep, goat, pig, and camel bones are also commonly used [10].

Bone Charcoal Production

The production process of bone charcoal involves the drying and baking of the raw bones in an oven under controlled oxygen concentrations to produce a porous medium with high surface area [1], [10]. The bones are then crushed into a small granular medium. Due to the complexity of bone charcoal production it is primarily produced at a single point and distributed throughout the surrounding region [10]. One such distribution hub for Kenya is the Catholic Diocese of Nakuru, Kenya (CDN).

The CDN produces a high quality, grayish-brown granular bone charcoal [9], [10]. The production process for bone charcoal at the CDN has four main steps: Charring, Crushing/Sieving, Washing, and Drying. The CDN has the kiln capacity to char ten tons of bones in one batch and the entire charring process takes 10 to 14 days [10]. The bones are baked for 1-5 days and then allowed to cool slowly for approximately a week. The temperature of the bones is continually measured at 14 different points through the bone mass and the airflow is adjusted accordingly [10]. The kiln is designed with grated floors and vertical grids to increase the airflow throughout the charring process. Altering the chimney size during the charring process controls the airflow and subsequently the temperature of the kiln. The bones are charred between 350 and 450°C for the majority of the charring period with maximum temperatures approaching 500°C near the end of the process [10]. The resulting charred bones are sorted by hand as either high or low quality by color. The high

quality bones are sent to the crushing facility while the low quality bones are recycled back into the charring process with the next batch.

The bones are then mechanically crushed and sieved to produce three granular sizes: Fine(<0.63mm), Middle(0.63-2mm) and Coarse(2-4mm) [10]. The middle and coarse fractions represent 60% of the production and are used in fluoride removal filters. The fine fraction is used in the production of the Calcium – Phosphate (CP) pellets and excess is sold as an additive for animal feed [9], [10].

The coarse and medium fractions then proceed in a series of 4 washing steps. The first step is used to remove any remaining organic impurities and involves the circulation of a 0.15 M NaOH solution through the bone mass. The second step is a rinsing with water to remove any residual NaOH from step 1. In step 3, the bone char is washed with carbonated water to reduce the pH below 8. Finally the bone char is rinsed with water to reduce the color and electrical conductivity of the effluent from the filter media. The entire washing process takes approximately three days [10]. The bone char is then dried for several days in the sun before packing in 60L bags to be sold to the local communities.

The CDN also offers a regeneration option for fluoride saturated bone char [9], [10]. The regeneration process begins by washing the fluoride-saturated bone char with a 1-2 M NaOH solution. Hydroxide and fluoride have a similar charge and atomic radii. It has been shown that increases in concentration of one species can shift the equilibrium between saturated bone char (Floroapatite, $Ca_5(PO_4)_3F$) and

bone (hydroxyapatite, $Ca_5(PO_4)_3OH$) [4], [10]. Therefore the same equilibrium process that facilitates the adsorption of fluoride allows for it's desorption. The regenerated bone char now continues the same washing procedure, as described above, for the newly produced bone char.

The effluent from the NaOH regeneration wash has a high fluoride concentration from the desorbed fluoride and is treated with calcium hydroxide ($CaOH_2$) and calcium chloride ($CaCl_2$) in batch to promote the precipitation of calcium fluoride (CaF_2) [10]. The CaF_2 precipitant is then captured in a sand filter to eliminate the reintroduction of the fluoride to the environment. To promote the bone char regeneration program, the CDN offers their unsaturated bone char at a 50% discount to those who bring used bone char to be regenerated [10].

Contact Precipitation

During the mid 1990s, investigations began into improving the bone charcoal adsorption process by the addition of calcium (commonly calcium chloride) and phosphate-containing (commonly monosodium phosphate) compounds to the fluoride contaminated influent water to promote the precipitation of calcium fluorite and floroapatite [1], [9]. This process is referred to as contact precipitation (CP). In initial laboratory batch studies, the CP addition to the adsorption process showed huge benefit, drastically improving the uptake capacity of the bone charcoal media. Although, when first implemented at the community level the process was deemed as too high maintenance due to the necessary addition of chemicals to the

influent stream [7], [8]. The CDN has since developed a calcium and phosphate-containing pellet, that that can be added to the adsorption column and will slowly dissolve releasing the required calcium and phosphate to promote the precipitation of CaF_2 and floroapatite.

The calcium and phosphate pellets are produced by mixing calcium hydroxide ($Ca(OH)_2$), fine bone char powder, and a locally available phosphate source in a concrete mixer [1]. The fine mixture is then sprinkled with water to promote pellet formation. The pellets are then allowed to dry and are distributed with the bone charcoal. The use of these pellets has been shown to increase the capacity of the filter 3-6 times as compared to bone char alone [8], [11], [12].

CHAPTER 2

EQUILIBRIUM STUDIES

The strength of an adsorbent is measured by its ability to remove the specified contaminant. This quantity, or adsorption capacity, is measured on a mass per mass basis such that the adsorption capacity of a given adsorbent is the mass of contaminant adsorbed per unit mass of adsorbent. Unit analysis may result in a unitless quantity but many times the adsorption capacity, q, is represented in units of mg/g or μg/g. The equilibrium adsorption capacity will vary for a specific contaminant with changes in contaminant concentration, adsorbent, pH, and temperature. Equilibrium adsorption capacity remains constant with changes in the quantity of adsorbent.

Isotherm Modeling

Information involving the adsorption process, the effects of the previously mentioned parameters, and the favorability of adsorption can be quantified using equilibrium isotherm modeling. Many named isotherms exist that describe the adsorption process. Each isotherm is characterized by a unique set of assumptions and operating parameters. Fitting experimental data to a wide range of isotherms allows for the appropriate isotherm(s) to be selected which best describe the specific adsorbent/adsorbate combination of interest. For this study of fluoride

adsorption to active alumina and bone charcoal five isotherms were selected for comparison including: Freundlich, Langmuir, Temkin, Harkins-Jura, and Halsey.

Freundlich Isotherm

The Freundlich isotherm is empirically derived and suitable for modeling adsorption on heterogeneous surfaces in dilute solutions [13]. Freundlich was the first to develop a mathematical model for adsorption onto solid surfaces and his equation currently remains as one of the most cited adsorption isotherms. The Freundlich isotherm is commonly seen in its condensed and linearized forms as shown in Equations 1 and 2 below [14]: $\boldsymbol{q_e = \frac{x}{m} = K_f C_e^{\frac{1}{n}}}$ Equation 1

$$\boldsymbol{Log\left(\frac{x}{m}\right) = LogK_f + \frac{1}{n}LogC_e} \quad \textbf{Equation 2}$$

Where,
q_e= equilibrium sorption capacity (mg/g)
K_f (mg adsorbate/g adsorbent) and n (g adsorbent/ L solution) are empirical constants (K_f >1 : Favorable Adsorption)
x/m = Mass of adsorbate per unit mass of adsorbent (mg/g)
C_e = Equilibrium Concentration of Adsorbate (mg/L)

Langmuir Isotherm

The Langmuir isotherm is a semi-empirical correlation for adsorption modeling [15]. Langmuir developed the correlation in 1916 using four main assumptions: (1) All adsorption sites are equal in energy, (2) Adsorbed molecules do not interact with each other, (3) Adsorption is limited to a monolayer, and (4) Desorption can occur.

The condensed and linearized forms of the Langmuir isotherm are shown in Equations 3 and 4 below[16]:

$$q_e = \frac{x}{m} = \frac{q_m K_L C_e}{1 + K_L C_e} \qquad \textbf{Equation 3}$$

$$\frac{1}{q_e} = \frac{m}{x} = \frac{1}{q_m K_L C_e} + \frac{1}{q_m} \qquad \textbf{Equation 4}$$

Where,
K_L (Liters of solution / mg of adsorbate) is an empirical constant
q_m (mg/g) is the theoretical maximum adsorption capacity for the system.

A dimensionless separation factor, R_L, for the Langmuir isotherm, as presented in Equation 5, provides a measure of the favorability of specific adsorbate/adsorbent systems. The reaction is termed favorable when $R_L < 1$ [17].

$$R_L = \frac{1}{1 + K_L C_i} \qquad \textbf{Equation 5}$$

Adsorption can be classified on a continuum from unfavorable, which is characteristic of little removal even at high concentrations to irreversible, which is characteristic of high removal at all concentrations. Favored adsorption will lead to greater removal of the adsorbate per unit mass of adsorbent resulting in greater adsorption efficiency, but higher difficulty of regeneration [18]. The favorability of adsorption is determined by the shape of the curve formed by its equilibrium adsorption capacity, q_e, versus initial adsorbate concentration C_i. The relationship between the favorability of adsorption and the shape of the curve on the q_e vs. C_i plot is shown in Figure 1 below.

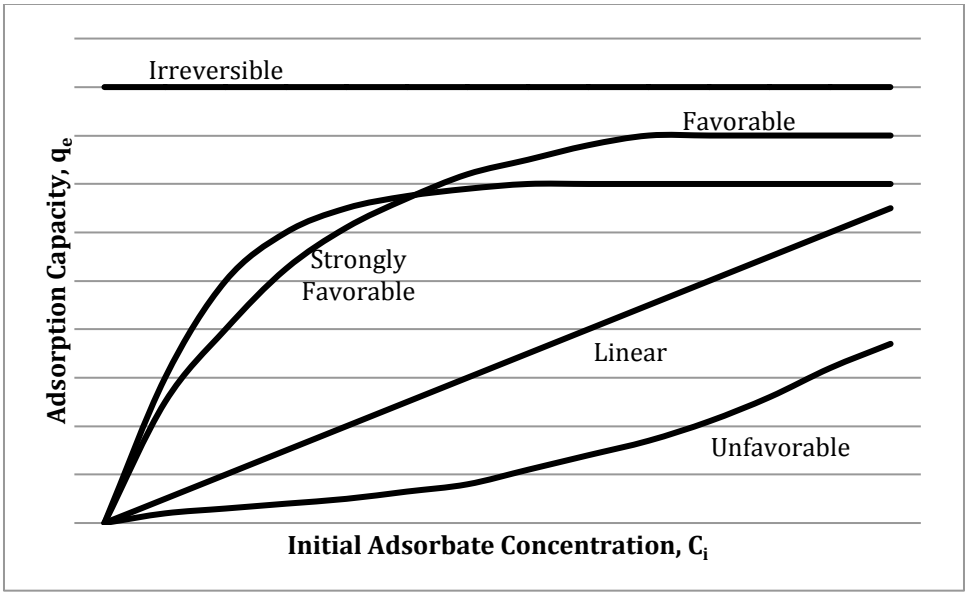

Figure 1. Graphical representation of favored adsorption

Temkin Isotherm

The Temkin isotherm is a thermodynamically based model that assumes the enthalpy of adsorption varies linearly with the concentration of the adsorbate [19], [20]. The Temkin isotherm is commonly used in its condensed and linearized forms as depicted in Equations 6 to 8 below [16]. The unitless constant B_1 is formed from the gas constant, temperature, and model constant for the Temkin isotherm and is related to the enthalpy of adsorption. Although related, the value of B_1 cannot be assumed to be equal in magnitude or sign to that of the ΔH_{abs}.

$$q_e = \frac{x}{m} = \frac{RT}{b}\ln(K_T C_e) \qquad \textbf{Equation 6}$$

$$q_e = \frac{x}{m} = B_1 \ln(K_T) + B_1 \ln(C_e) \qquad \textbf{Equation 7}$$

$$B_1 = \frac{RT}{b} \qquad \textbf{Equation 8}$$

Where:
R = universal gas constant (8.314 J/(mol K))
b = model constant (J/mol)
T = absolute temperature (K)
K_T = equilibrium binding constant, and
B_1 = unitless constant related to the enthalpy of adsorption.

Harkins-Jura and Halsey Isotherms

The Harkins-Jura and Halsey Isotherms account for the possibility of multi-layer adsorption and heterogeneous pore distribution and are represented in their linearized forms as shown in Equations 9 an 10 [16]. The Harkins-Jura Isotherm has been used to effectively model the adsorption of red dye on tea waste [21], fluoride on activated alumina [16], and crystal violet dye on watermelon rind [22]. The Halsey isotherm has been shown to display a good description of fluoride adsorption on Activated Alumina [16], red dye on tea and palm kernel waste [21], [23].

Harkins-Jura:

$$\frac{1}{q_e^2} = \left(\frac{B}{A}\right) - \left(\frac{1}{A}\right)\log(C_e) \qquad \textbf{Equation 9}$$

Halsey:

$$\ln(q_e) = \left[\left(\frac{1}{n_H}\right)\ln(k)\right] - \left(\frac{1}{n_H}\right)\ln\left(\frac{1}{C_e}\right) \qquad \textbf{Equation 10}$$

Where:
A, B, k, and n_H are empirical constants.

Review of Fluoride Adsorption

Fluoride adsorption on activated alumina and bone char has been studied and the affects of critical system variables on the adsorption capacity have been

documented. These studies documented that varying the pH of the solution had drastic effects on the equilibrium adsorption capacity of the adsorbent with optimum pH ranging from 3 to 5 [24], [25]. The adsorption capacity of the bone char varied from 3 to 7 mg/g over a pH range of 7 to 4.6 respectively [24] and 3 to 10 mg/g over a pH range of 7 to 3 respectively [25]. The temperature of the system was also shown to have a much smaller effect than pH, showing little to very moderate change (±0.3 mg/g) over a practical range of temperatures (10 -40°C) [25]. Physical surface area of the adsorbate has also been shown to have little effect on the adsorption capacity of bone char. The adsorption capacity of the bone char does show a slight, non-proportional rise with increases in surface area [25]. This is suggested to be a product of the smaller particles containing less blocked pores that are unavailable for adsorption and not due to a change in specific surface area of the bone char.

Multiple studies have shown that the Freundlich and Langmuir isotherms adequately characterize equilibrium fluoride adsorption on bone char and activated alumina [16], [24–30]. The Halsey [16], Redlich-Peterson [29], Temkin [16], [29], and Prausnitz-Radke [26] isotherms have also been shown to model the system with varying degrees of success. The adsorption of fluoride on various adsorbents is commonly well described by several isotherms and the individual experimental conditions are responsible for one or more isotherms displaying the “best” fit to the system. All studies demonstrated the basic batch adsorption theory of an increased

initial concentration of adsorbate resulting in higher equilibrium concentrations but also higher adsorption capacities for the adsorbent.

Experimental Methods

The concentration of fluoride in solution was measured using a Cole-Parmer replaceable membrane, fluoride ion-selective electrode (ISE) model number YO-27506-30. The output voltage of the ISE was measured using the accumet model 25 two-channel ion meter and the probe was calibrated with fluoride standards in the appropriate range for the fluoride concentrations to be measured. The electrode was calibrated every hour as suggested by the manufacturer such that the measurement error can be assumed as to be ±2% of reading. The square of the Pearson's correlation coefficient, R^2, for the calibration line of best fit was ensured to be greater than 0.999. The solutions were prepared by the addition of a total ionic strength adjustment buffer (TISAB) reagent tablet (Cole-Parmer EW-99359-31) to each 40 mL sample to be analyzed. The solutions were measured at the same temperature as the probe calibration to reduce any additional error from temperature differences. The TISAB reagent is used to buffer the pH of the solution to a pH of 5.0 to 5.5, which reduces the interference from the hydroxide ion. The TISAB also breaks any complexes formed between fluoride and hydrogen, aluminum, silicon, or iron (III). Anions such as carbonate and phosphate and most cations do not directly interfere with the probe operation but may show indirect effects by increasing the hydroxide ion concentration.

Simultaneously Stirred Reactor Description

The Activated Alumina batch studies were completed using a commercially available sample of SIR-900 from ResinTech, Inc. The batch system consisted of 6 simultaneously-stirred 1-liter beakers into which varying concentrations of sodium fluoride (ACROS Organics Lot Number: A0292917) contaminated water (800 mL, 7 to 32 ppm F^-) and SIR-900 were added. The solution was prepared using deionized water and the system pH was maintained near 5.40 with an acetic acid/acetate buffer. A Phipps and Bird stirrer (Model number: 7790-400) was fitted with stainless steel paddle stir plates and operated at 150 revolutions per minute for the entire study. The concentration of fluoride in solution was measured and recorded throughout the study starting a ten minute intervals and gradually increasing as the adsorption rate slowed. The effects of evaporation on the open beakers was measured and accounted for in adsorption calculations. A schematic of the batch system is shown in Figure 2.

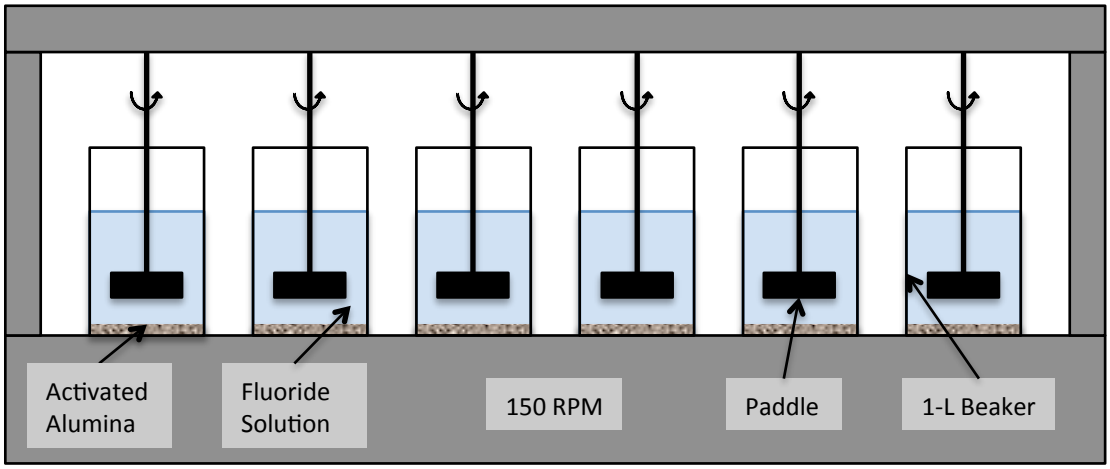

Figure 2. Schematic of Activated Alumina Simultaneously-Stirred Batch System

Differential Volume Reactor Description

The Bone Char and contact precipitation (CP) batch studies were conducted using a differential volume reactor (DVR). The bone charcoal and CP pellets were obtained directly from the Catholic Diocese of Nakuru, Kenya (CDN) in the summer of 2010. Three size fractions (fine, medium, and course) of bone char were available. The CP pellets varied in size and were sifted to obtain a size range between 0.84 mm and 3.36 mm for use in all differential volume batch studies. The DVR system consisted of a peristaltic pump (Cole-Parmer model number: 7553-80) and column made of ¾-inch clear plastic tubing arranged to operate in a closed, up-flow fashion. The differential volume of adsorbent was supported above and below using plastic craft beads. When a mixture of both bone char and CP pellets were studied in the DVR, the CP pellets were placed below the bone char such that the upward flowing water would contact the pellets before the bone charcoal. The flow of fluoride contaminated water through the system remained constant at 100 mL per minute. The fluid reservoir was configured with a two-hole rubber stopper to allow the pump influent and effluent to be cycled through the reservoir. The pump intake tube was placed near the bottom of the reservoir while the return tube was placed four inches above the water level to promote mixing of the solution. The reservoir contained of 500 mL of stock solution, which gave the system a recycle time of five minutes at the specified flow rate.

A schematic of the DVR system is shown in Figure 3. The fluoride solutions were prepared via dilution with deionized water from a stock 1000 ppm sodium fluoride solution. To take fluoride measurements the reservoir was shaken to completely mix the solution, and a 40 mL aliquot was added to one TISAB tablet. After the measurement was recorded, the sample and dissolved tablet were returned to the reservoir.

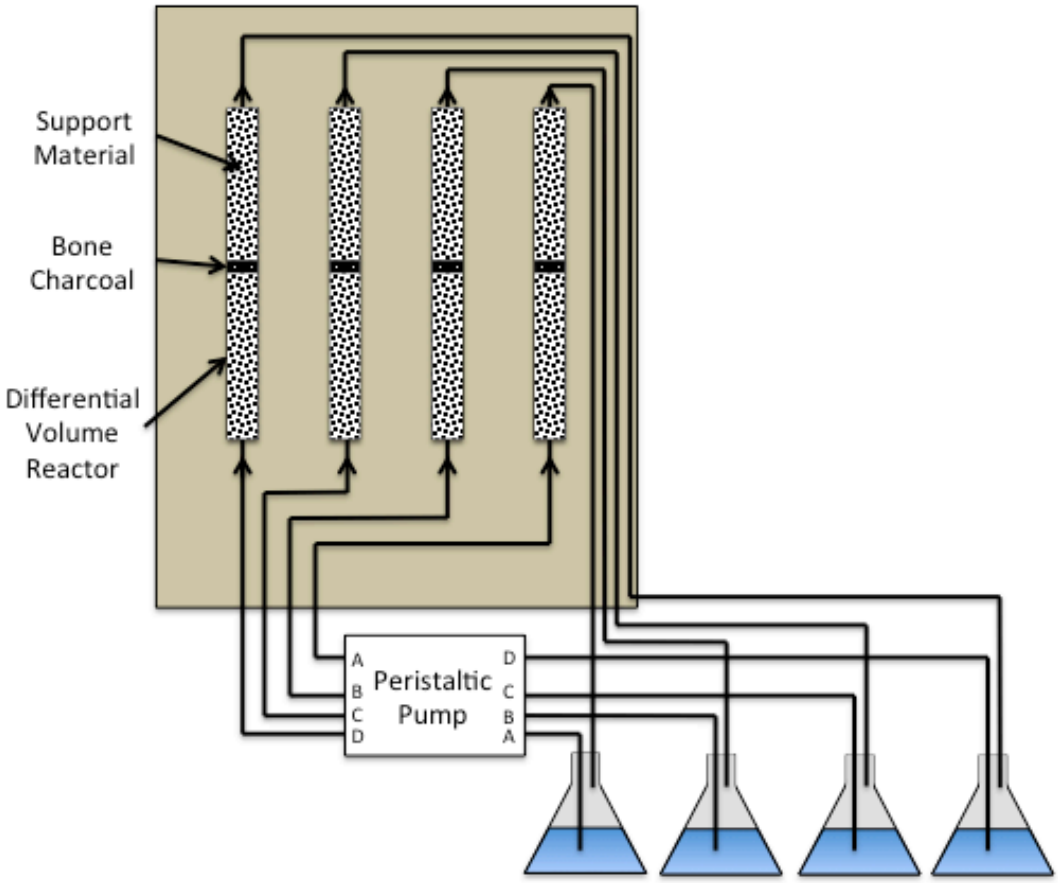

Figure 3. Schematic of Differential Volume Reactor

Experimental Results using Activated Alumina – Equilibrium Modeling

The equilibrium adsorption capacity of fluoride for the Resin Tech SIR-900 activated alumina is linearly dependent, R^2= 0.996, on the concentration of fluoride in solution for the fluoride concentrations tested (7 to 32 ppm F^-). Figure 4 displays the chart of equilibrium adsorption capacity, q_e, versus initial fluoride concentration, C_i, for the range tested. The linear correlation corresponds to linear favorability represented in Figure 1.

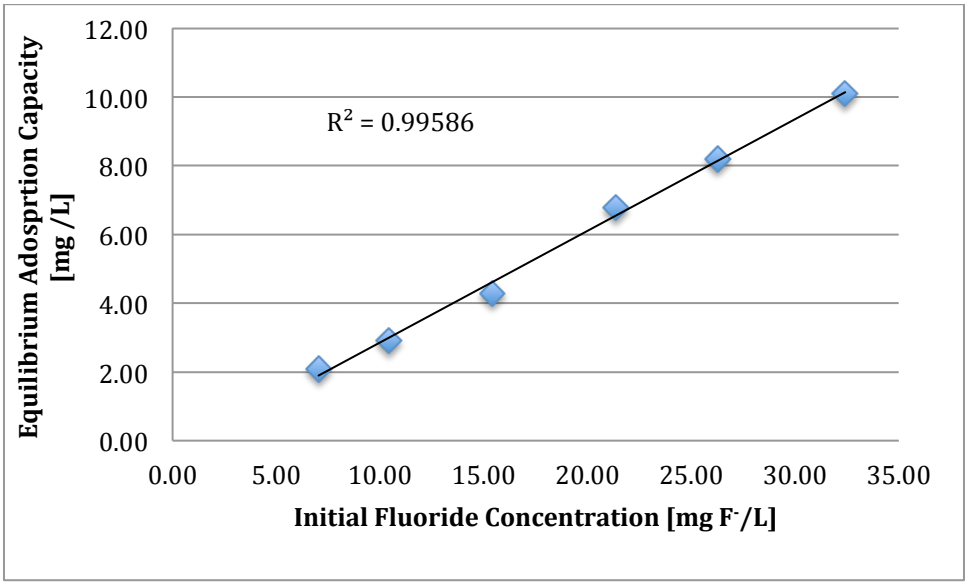

Figure 4. Adsorption capacity versus initial adsorbate concentration for activated alumina.

Isotherm Modeling

The equilibrium fluoride adsorption data for bone char and activated alumina were fitted to the five isotherms described previously. Coefficients of determination, R^2, were found for each isotherm. For the activated alumina trials, all but one isotherm evaluated described equilibrium adsorption extremely well with R^2 values

indicative of good linear fit (R^2>0.9). Experimental results were described reasonably well by the Temkin isotherm; the correlation coefficient was R^2 = 0.82. The Harkins-Jura and Langmuir isotherms best described the adsorption system, with R^2 values of 0.93 and 0.92, respectively. The isotherm plots are presented below in Figures 5 to 9.

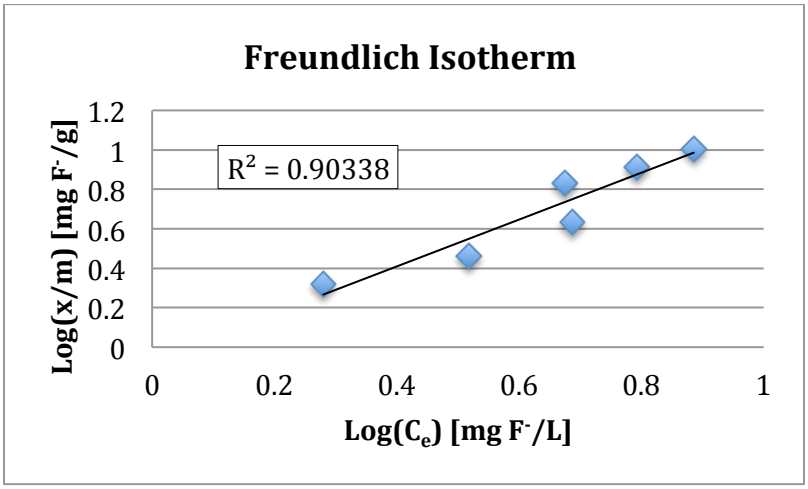

Figure 5. Freundlich isotherm for fluoride adsorption on activated alumina.

Using linear regression analysis, the Freundlich empirical constants, n and K_f, were determined to be 0.84 and 0.85 respectively. A K_f value less than one and a 1/n value greater than one is indicative of unfavorable adsorption for the activated alumina/fluoride system.

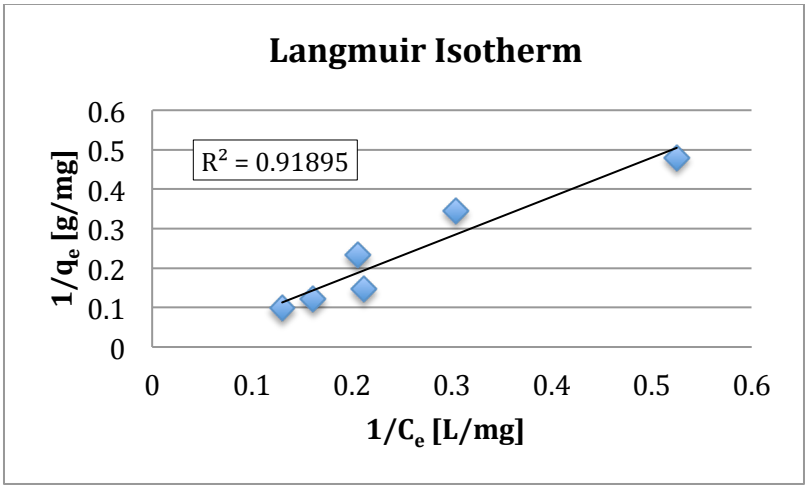

Figure 6. Langmuir isotherm for fluoride adsorption on activated alumina.

The empirical constants for the Langmuir isotherm, K_L and q_m, were found to be -0.016 L/mg and -62.11 mg/g, respectively. These values allow for the calculation of a R_L value for various initial concentrations of fluoride. The R_L values for initial concentrations studied are presented in Table 1 below.

Table 1. Langmuir Separation Factor, R_L, values for Activated Alumina Study

Initial Concentration, C_i (mg F^-/L)	Dimensionless Separation Factor, R_L
7.0	1.13
10.4	1.20
15.4	1.33
21.4	1.53
26.3	1.74
32.4	2.11

Despite Figure 4 indicating predominantly linear favorability, the calculated R_L values slightly greater than one are indicative of slightly unfavorable adsorption.

The results presented above indicate that as initial concentration of fluoride is increased, the adsorption becomes less favorable.

The Temkin constants, B_1 and K_T, are found to be 5.76 and 0.62, respectively. The constant B_1, is related to the heat of adsorption, ΔH_{abs}, although its sign cannot be simply interpreted as the sign of ΔH_{abs} for the adsorbent/adsorbate relationship. Having the lowest linear correlation out of the isotherms presented the Temkin isotherm, Figure 7, was not considered as a good descriptor of fluoride adsorption on activated alumina.

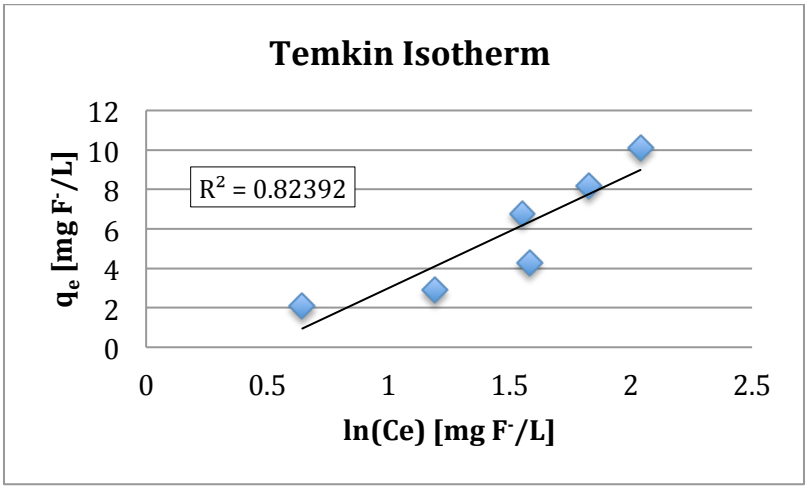

Figure 7. Temkin isotherm for fluoride adsorption on activated alumina.

The empirical constants, A and B, for the Harkins-Jura Isotherm at 25°C were found to be 2.6 and 0.83, respectively. Table 2 below summarizes the Harkins-Jura empirical constants from the literature. The magnitude of the constants is shown to vary greatly according to the adsorbate/adsorbent combination and temperature of adsorption.

Table 2. Harkins-Jura isotherm empirical constants presented in literature

Temperature °C	A	B	Adsorbate/Adsorbent	Source
88 °C	59.88	1.916	Fluoride/Activated Alumina	[16]
36 °C	149.25	1.642	Congo Red Dye/ Palm Kernel Coat	[23]
30 °C	200.55	1.3504	Red Dye/ Tea Waste	[21]
40 °C	215.15	1.3189	Red Dye/ Tea Waste	[21]
50 °C	252.46	1.3038	Red Dye/ Tea Waste	[21]
30 °C	14.70	0.35	Crystal Violet Dye / Watermelon Rind	[22]
40 °C	10.10	0.13	Crystal Violet Dye / Watermelon Rind	[22]
50 °C	25.64	0.30	Crystal Violet Dye / Watermelon Rind	[22]

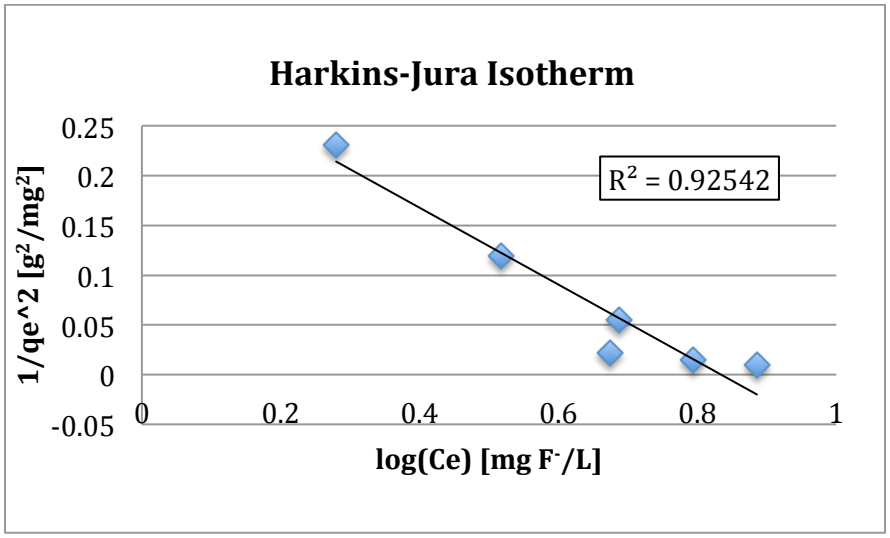

Figure 8. Harkins-Jura isotherm for fluoride adsorption on activated alumina.

The empirical constants, n_H and k, for the Halsey isotherm are found to be 0.84 and 0.88, respectively.

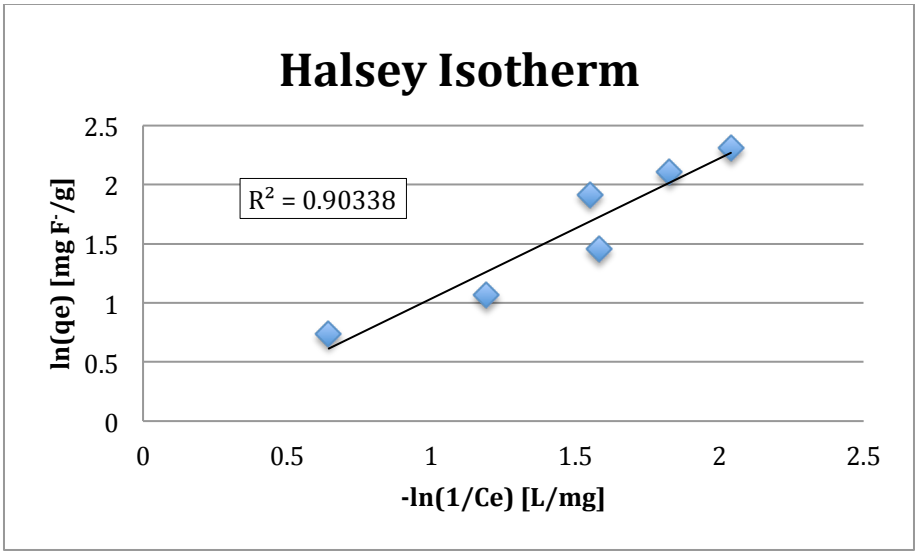

Figure 9. Halsey isotherm of the adsorption of fluoride on activated alumina.

Experimental Results using Bone Char – Equilibrium Modeling:

The equilibrium adsorption capacity, q_e, for the adsorption of fluoride onto bone char was shown to increase with increases in the initial fluoride concentration. This data, displayed in Figure 10, when fit with a linear trend line is found to have an R^2 value of 0.950, but when fit to a second-order polynomial equation the line of best fit displays an improved $R^2 = 0.998$. The best linear regression from the second-order polynomial illustrates the slight concave downward trend, which is indicative of slightly favored adsorption.

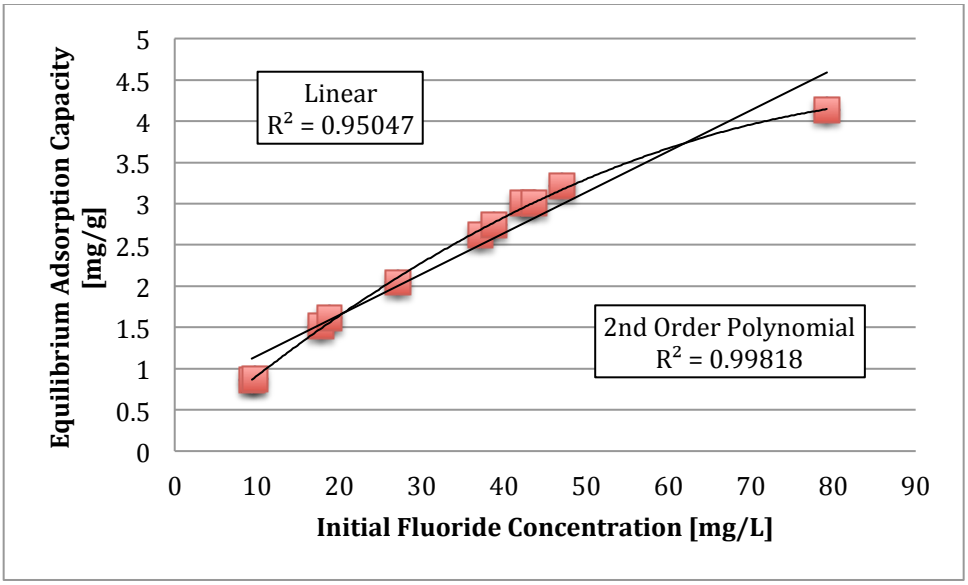

Figure 10. Adsorption capacity of bone char for various initial fluoride concentrations.

Isotherm Modeling

For experiments using bone char as the adsorbent, all of the isotherms investigated, with the exception of the Harkins-Jura Isotherm, modeled system behavior well with R^2 values greater than 0.9. The Halsey and Freundlich isotherms both described the experimental data the best with R^2 values above 0.93. All the isotherm plots for the fluoride/bone char system are shown in Figures 11 through 15 below.

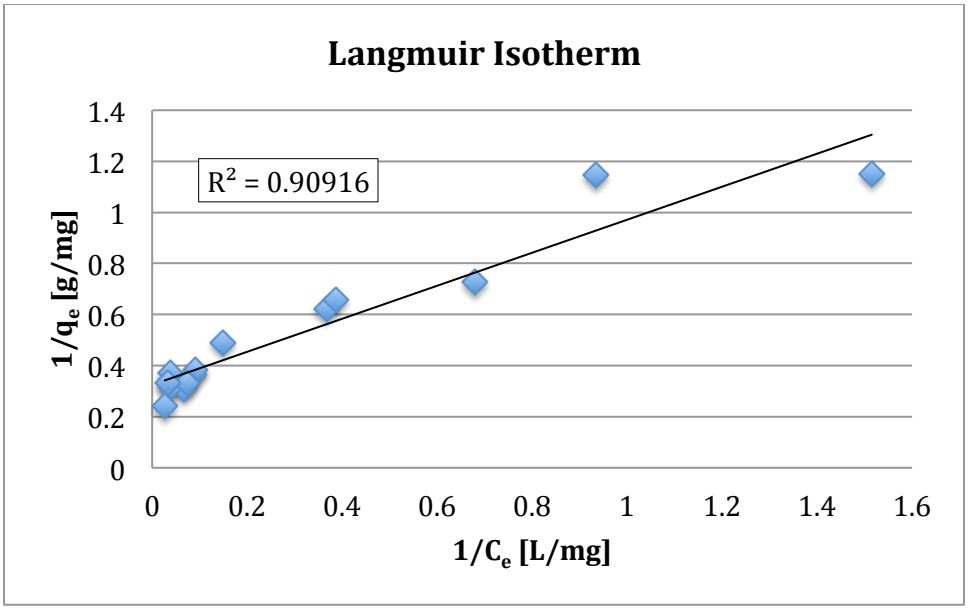

Figure 11. Langmuir adsorption isotherm for fluoride on bone char.

The Langmuir constants, K_L and q_m, were determined to be 0.50 L/mg and 3.08 mg/g respectively. The constant q_m represents the maximum possible adsorption capacity for the system. The data above in Figure 10 shows that this maximum capacity was exceeded at high initial concentrations and if the second-order polynomial trend line is assumed to hold at higher initial concentrations it predicts a maximum adsorption capacity of 4.73 mg F^-/L at concentrations higher than 105 mg F^-/L, resulting in a percent difference of 54% from the Langmuir isotherm predicted maximum capacity. Using the K_L value and the initial concentrations for the trials represented above, the Langmuir separation factor was calculated to determine the favorability of the adsorption of fluoride on bone char. The results are summarized in Table 3 below.

Table 3. Langmuir separation factor, R_L, values for adsorption of fluoride on bone char.

Initial Concentration, C_i (mg/L)	R_L
9.35	0.175
9.71	0.170
9.78	0.169
17.76	0.101
18.79	0.096
27.13	0.068
28.96	0.064
37.12	0.051
37.14	0.051
38.78	0.049
42.24	0.045
43.70	0.044
47.05	0.041
57.20	0.034
79.22	0.024

Adsorption is deemed favored for R_L values less than one. Table 3 shows that for the adsorption of fluoride on to bone char the adsorption is always favored for the initial concentrations tested. This observation fits with the concave downward trend seen in Figure 10. Table 3 also indicates that the higher the initial fluoride concentrations the more favored the adsorption will be.

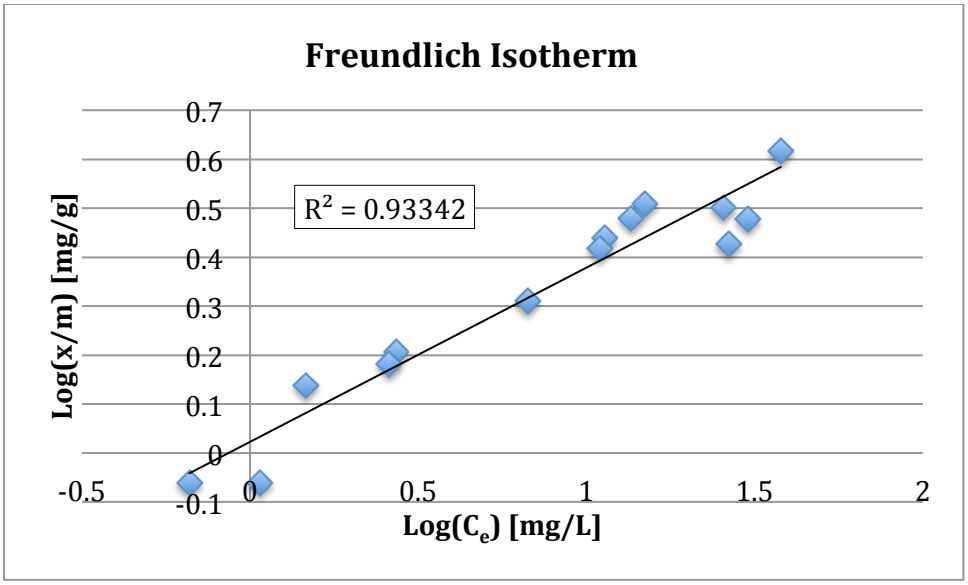

Figure 12. Freundlich adsorption isotherm for fluoride on bone char

The Freundlich empirical constants K_f and n were determined to be 1.05 mg/g and 2.81 L/g, respectively. The K_f value greater than one supports the determination of favorable adsorption of fluoride on bone char.

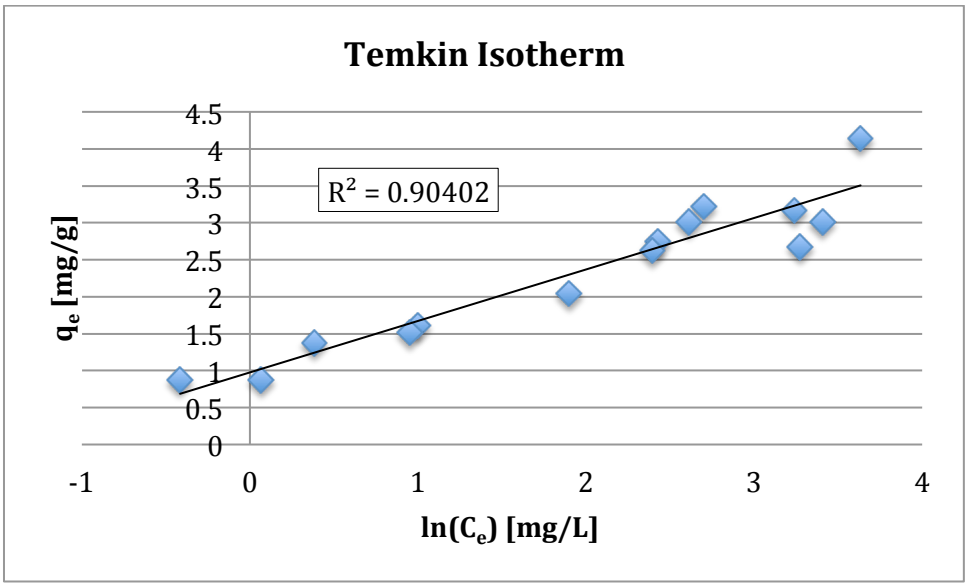

Figure 13. Temkin adsorption isotherm for fluoride on bone char.

The Temkin equilibrium binding constant, K_T, and empirical constant related to ΔH_{ads}, B_1, were found to be 4.06 mg/g and 0.70 respectively.

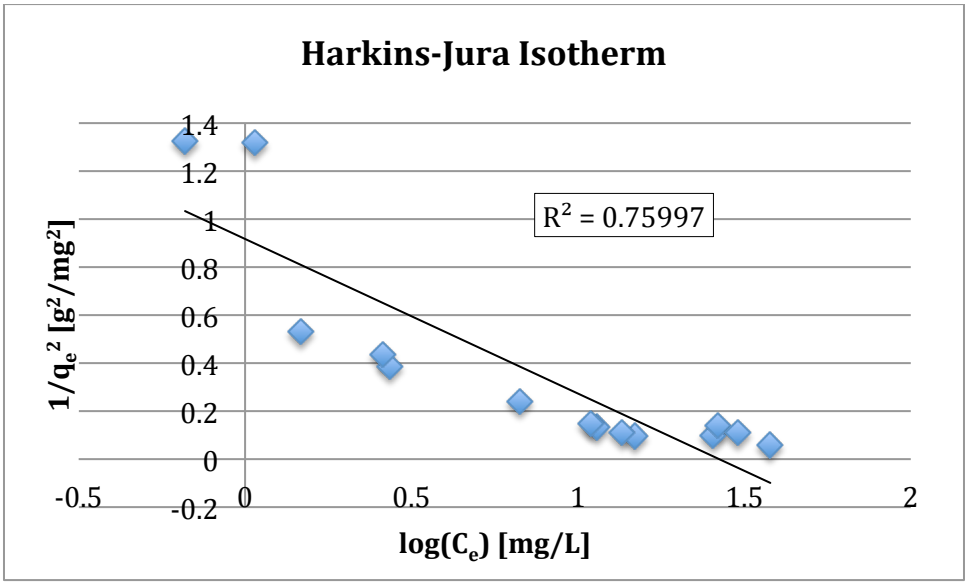

Figure 14. Harkins-Jura adsorption isotherm for fluoride on bone char.

Harkins-Jura constants A and B were found to be 1.55 and 1.42, respectively.

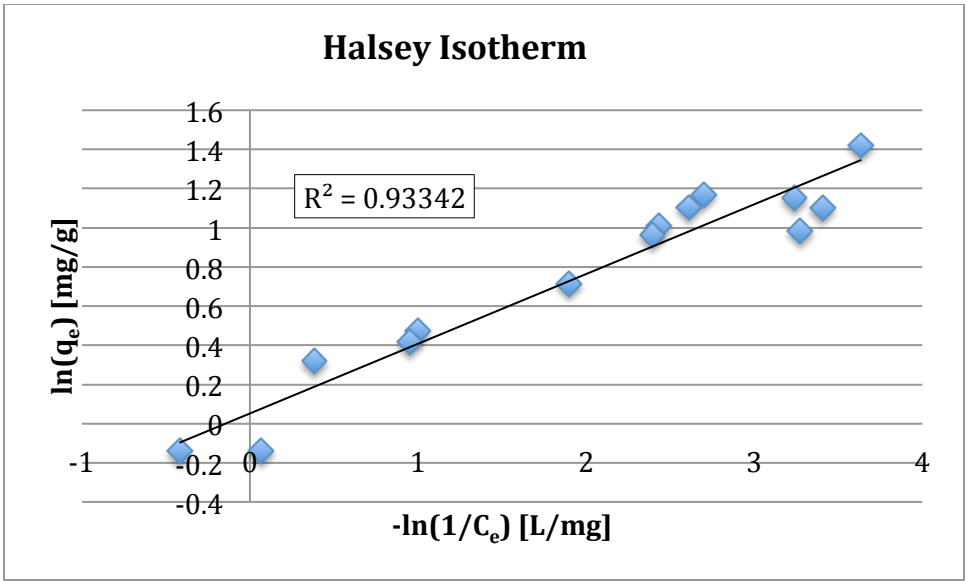

Figure 15. Halsey adsorption isotherm for fluoride on bone char

Halsey constants n_H and k were found to be 2.81 and 1.16, respectively.

Table 4 summaries the various isotherms, their plotted axes, associated R^2 values, and constants for the bone char and activated alumina equilibrium isotherm data.

Table 4. Summary of adsorption isotherms

Isotherm	Plotted Axes (Y vs. X)	R^2 Activated Alumina	R^2 Bone Char	Constants Activated Alumina	Constants Bone Char
Langmuir	$\frac{1}{q_e}\ vs. \frac{1}{C_e}$	0.90	0.91	K_L=0.016 q_m=-62.1	K_L=0.50 q_m=3.08
Freundlich	$\log(q_e)\ vs. \log(C_e)$	0.92	0.93	K_f=0.85 n=0.84	K_f=1.05 n=2.81
Temkin	$q_e\ vs. \ln(C_e)$	0.82	0.90	K_T=0.62 B_1=5.76	K_T=4.06 B_1=0.70
Harkins-Jura	$\frac{1}{q_e^2}\ vs. \log(C_e)$	0.93	0.76	A=2.6 B=0.83	A=1.55 B=1.42
Halsey	$\ln(q_e)\ vs. -\ln(\frac{1}{C_e})$	0.90	0.93	k=0.88 n_H=0.84	k=1.16 n_H=2.81

CHAPTER 3

KINETICS MODELING

Modeling adsorption with isotherms allows for a better understanding of the factors that affect equilibrium and maximum adsorption capacity for a particular system. However, equilibrium isotherms do not provide information about the time response or kinetics of the system. An understanding of adsorption kinetics is important to system design parameters such as residence time, which dictate the physical size and flow rates for many unit operations. The kinetics of physical and chemical reactions can be described by a series of models including: Pseudo-first-order, Second-order, Pseudo-second-order, and Elovich models.

Kinetics Models

Pseudo-First-Order

Lagergren was first to develop and publish a rate equation to describe the kinetics of adsorption from a liquid phase onto a solid adsorbent [31]. The first-order relationship was developed while studying the adsorption of two organic acids (oxalic and malonic acid) onto charcoal. Lagergren's first-order rate equation, presented below, is most commonly referred to as a Pseudo first-order rate equation. The term 'pseudo' is applied to differentiate rate equations using

adsorption capacities, q, from other first-order equations using liquid phase concentrations, C.

$$\frac{dq_t}{dt} = k_1(q_e - q_t) \qquad \textbf{Equation 11}$$

In Equation 11, k_1 is a first-order rate constant with units of inverse time and q_e and q_t are the adsorption capacity of the adsorbent at equilibrium and time t, respectively. Integration, with boundary conditions of $q_t(t=0)=0$ and $q_t(t=t)=q_t$, will result in the commonly used linear form shown as Equation 12.

$$\log(q_e - q_t) = \log(q_e) - \frac{k_1 t}{2.303} \qquad \textbf{Equation 12}$$

The pseudo first-order rate reaction has been used to study the adsorption of various dyes onto activated carbon [31] and TiO_2 [32]. It has also been applied to the adsorption of heavy metals on rice husk [33], and fluoride onto activated alumina [34] and bone char [16].

Pseudo-Second-Order

A pseudo second-order rate equation for adsorption from a liquid to a solid phase was originally developed in 1995 by Ho[35]. The pseudo second-order rate equation was developed while studying the adsorption of divalent metal cations on sphagnum peat moss. Again the term 'pseudo' is applied to indicate the use of adsorption capacity as opposed to concentration in the second-order rate equation. The differential form of Ho's equation is given as Equation 13 below.

$$\frac{dq_t}{dt} = k_{2s}(q_e - q_t)^2 \qquad \textbf{Equation 13}$$

In Equation 13, k_{2s} is the pseudo second-order rate constant with units of $q^{-1}t^{-1}$. Integration with boundary conditions of $q_t(t=0)=0$ and $q_t(t=t)=q_t$, results in Equation 14, the linearized form of the second-order rate equation.

$$\frac{t}{q_t} = \frac{1}{k_{2s}q_t^2} + \frac{t}{q_e} \qquad \textbf{Equation 14}$$

Second-Order

Equation 15 below, presents a more conventional second-order rate equation in differential form.

$$\frac{dC_t}{dt} = -k_2 C_t^2 \qquad \textbf{Equation 15}$$

Where, k_2 is the second-order rate constant with units of $C^{-1}t^{-1}$ and C_t is the liquid phase concentration at time, t. Integration with boundary conditions of $C_t(t=0)=0$ and $C_t(t=t)=C_t$, will yield Equation 16 the linearized form of the second-order rate equation.

$$\frac{1}{C_t} = k_2 t + \frac{1}{C_0} \qquad \textbf{Equation 16}$$

Where C_0 is the initial concentration at time t=0.

Elovich

Tamman and Koster first presented the Elovich equation in 1922 [36] although considerable advances to the equation were made in 1934 by Zeldowitsch to describe the chemisorption of carbon monoxide on manganese dioxide [37], [38] and in 1939 by Elovich and Zhabrova [39]. The name “Elovich” was retained and

continues to be referenced to keep consistent with past literature [40]. The Elovich equation appropriately describes an adsorption process when the adsorption rate decreases exponentially with a decrease in the number of available adsorption sites. The differential form of the Elovich equation is presented in Equation 17 below:

$$\frac{dq_t}{dt} = \alpha e^{(-\beta q_t)} \qquad \textbf{Equation 17}$$

Where, β is a desorption constant and α is the initial adsorption rate such that the adsorption rate, $\frac{dq_t}{dt}$, is equivalent to α when the adsorption capacity at time t, q_t, is zero. Assuming that αβ>>1 and integrating with the boundary conditions of $q_t(t=0)=0$ and $q_t(t=t)=q_t$ will result in the linearized form as shown in Equation 18.

$$q_t = \frac{\ln(t)}{\beta} + \frac{\ln(\alpha\beta)}{\beta} \qquad \textbf{Equation 18}$$

Such that a graph of q_t versus ln(t) will result in a straight line correlation from which the α and β constants can be derived. The Elovich equation has been shown to have good fit to many adsorbate/adsorbent systems including: Phenol on activated carbon [41], Fluoride removal by activated alumina [16], Metal ions on solvent impregnated resins [42], and Cadmium on bone char [43].

The differential and linear forms of the kinetics models presented above are summarized in Table 5 below along with the appropriate axes for the straight-line plot.

Table 5. Summary of Kinetics Models

	Differential Form	Linear Form	Plot (y vs. x)
Pseudo-first-order	$\frac{dq_t}{dt} = k_1(q_e - q_t)$	$\log(q_e - q_t) = \log(q_e) - \frac{k_1 t}{2.303}$	$\log(q_e - q_t)\ vs. t$
Second-order	$\frac{dC_t}{dt} = -k_2 C_t^2$	$\frac{1}{C_t} = k_2 t + \frac{1}{C_i}$	$\frac{1}{C_t}\ vs. t$
Pseudo-second-order	$\frac{dq_t}{dt} = k_{2s}(q_e - q_t)^2$	$\frac{t}{q_t} = \frac{1}{k_{2s} q_t^2} + \frac{t}{q_e}$	$\frac{t}{q_t}\ vs. t$
Elovich	$\frac{dq_t}{dt} = \alpha e^{(-\beta q_t)}$	$q_t = \frac{\ln(\alpha\beta)}{\beta} + \frac{\ln(t)}{\beta}$	$q_t\ vs. \ln(t)$

Presentation of Kinetics Data

Activated Alumina

The kinetics data for the adsorption of fluoride on activated alumina and bone char was described using the four models summarized in Table 5. Coefficients of determination, R^2, were found to determine which of the models provided the best description for the particular system. The pseudo second-order and Elovich models displayed the highest R^2 values for the activated alumina trials. For these trials, the initial fluoride concentrations were varied from 7 to 15ppm F^- with the higher concentrations displaying the highest R^2 values for the respective models. Figures 16 to 19 present the activated alumina kinetics data for the four models chosen for this study.

The pseudo first-order plot, Figure 16, demonstrates high R^2 values (Average R^2 = 0.941) to the linear regression trend line, but a visual assessment of fit reveals a

concave upward curvature to the data. These non-linear attributes and lower mean R^2 values than Pseudo Second-Order (Average R^2 = 0.992) and Elovich (Average R^2 = 0.976) models indicate that the process cannot be best described by a first-order system.

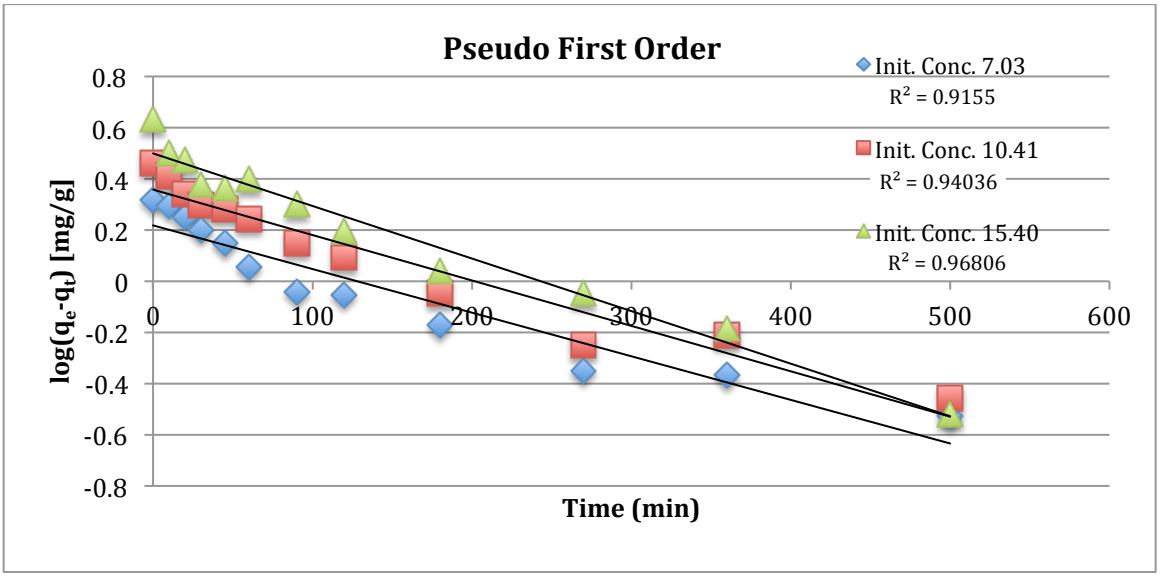

Figure 16. Pseudo First-order plot for adsorption of fluoride on activated alumina

The second-order plot, Figure 17, displays the lowest fit to the linear regression trend line out of all kinetics models tested. The average R^2 value for the three concentrations presented is R^2 = 0.816 indicating a poor description for the activated alumina/fluoride adsorption system.

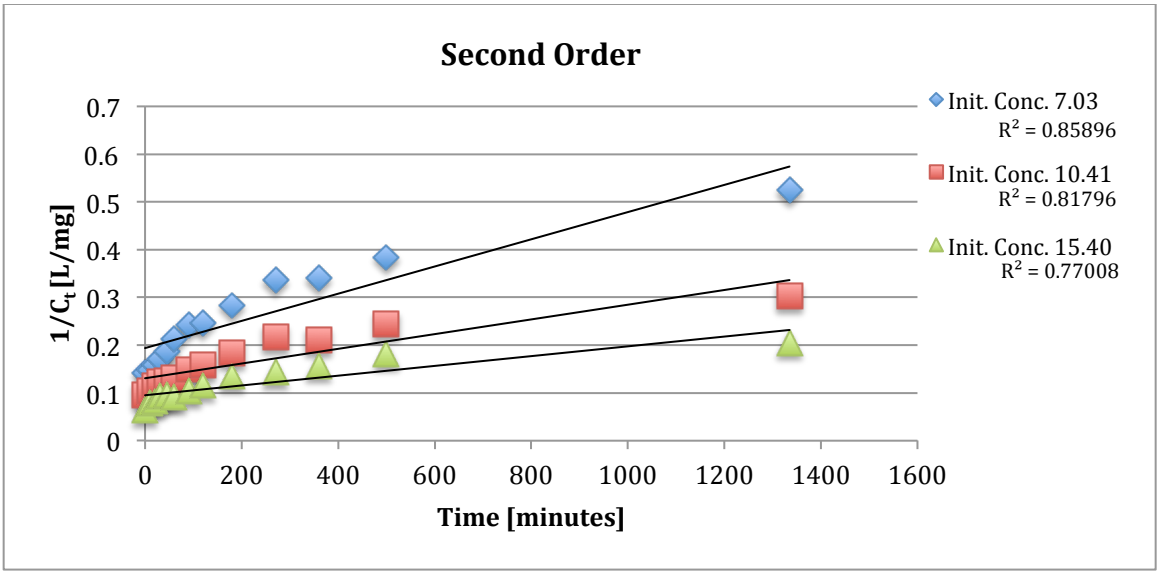

Figure 17. Second-order plot for adsorption of fluoride on activated alumina

All initial fluoride concentrations were indicative of a linear correlation when fitted with the pseudo second-order and Elovich models. The pseudo second-order model showed a slightly better fit to the linear trend line, (Average $R^2 = 0.992$ vs. Average $R^2 = 0.976$). The Elovich model plot shows the data points wavering above and below the linear best fit line indicating accuracy of the model but some instrumental uncertainty and indeterminate error from the fluoride concentration measurements.

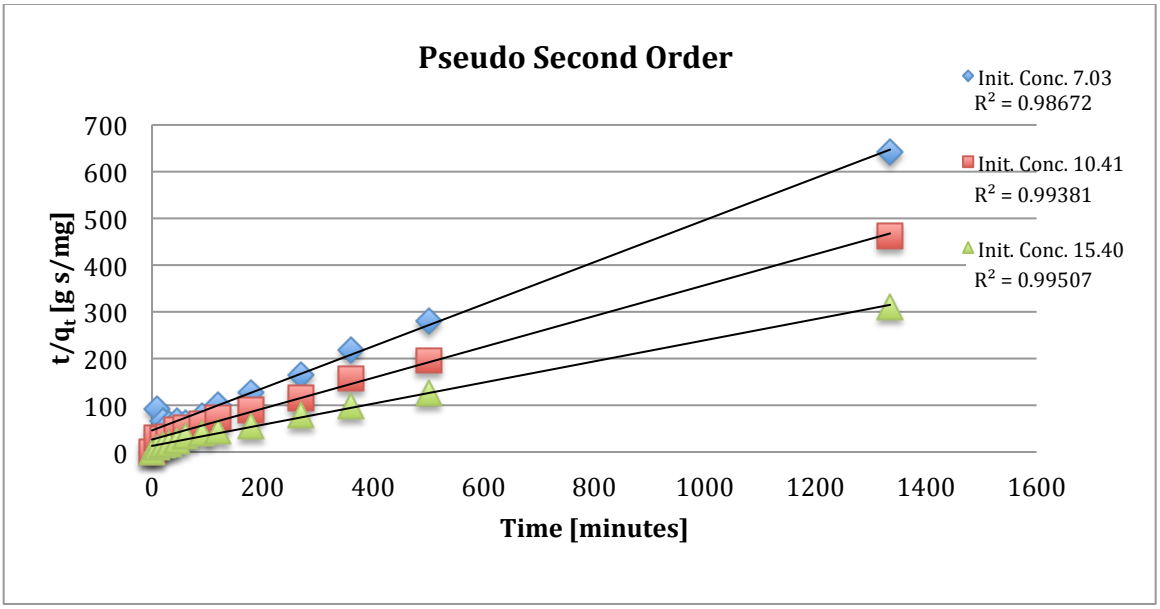

Figure 18. Pseudo Second-order plot for adsorption of fluoride on activated alumina

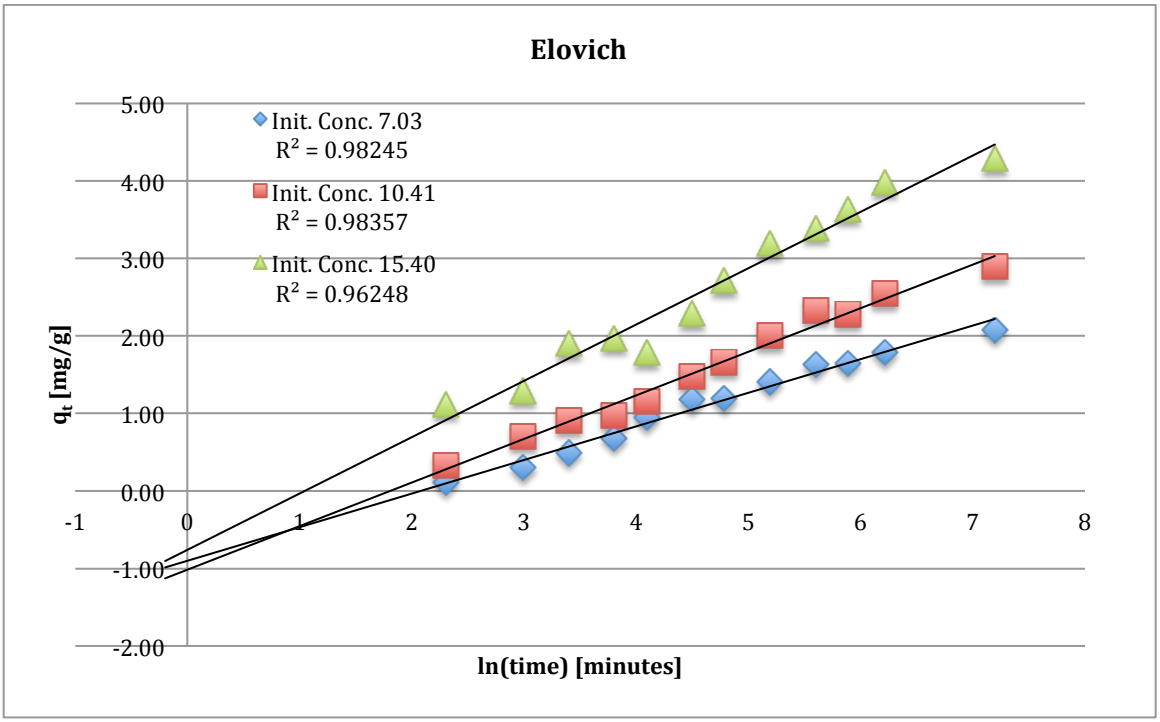

Figure 19. Elovich plot for adsorption of fluoride on activated alumina

The linear correlation in the Elovich plot suggests that the sorption of fluoride on activated alumina has a substantial chemisorption component and the adsorption rate is exponentially dependent on the number of available adsorption sites.

Bone Char

The kinetic modeling results for fluoride adsorption on bone char are presented below in Figures 20 to 23. Although high R^2 values indicate good linear fit, a visual assessment of fit for the pseudo first-order plot to the linear trend line shows a poor correlation to the model due to an observed concave upward curvature in the data points.

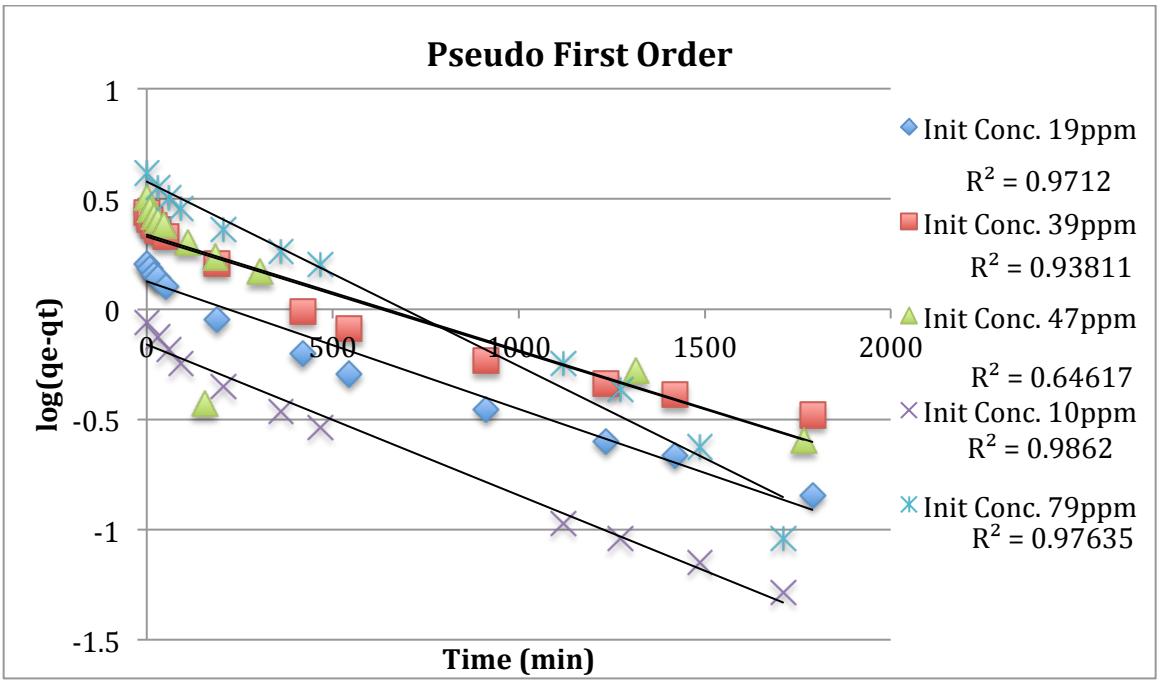

Figure 20. Pseudo First-order plot for adsorption of fluoride on bone char

The second-order model is a good representation of the adsorption system at low concentrations. Initial concentrations less than twenty ppm show high correlation with the linear trend line for the entire adsorption time. Also, trials with higher initial concentration demonstrate good linear fit after the concentration of the solution, C_t, falls below twenty ppm.

Figure 21. Second-order plot for adsorption of fluoride on bone char

The pseudo second-order and Elovich models again showed the best description for the adsorption of fluoride. Both models demonstrated high coefficients of determination ($R^2 \geq 0.98$) for all initial concentrations tested. The Pseudo second-order model displays a linear fit for the data at concentrations less than approximately 35 ppm. At concentrations higher than 35 ppm, variance from the line of best fit is shown. As the fluoride is adsorbed, the solution concentration at

time t, C_t, is reduced and the data points again configure to a linear configuration. The Elovich model showed good linear characteristics over all fluoride concentrations tested indicating that the Elovich model provides the best description of fluoride adsorption on bone char.

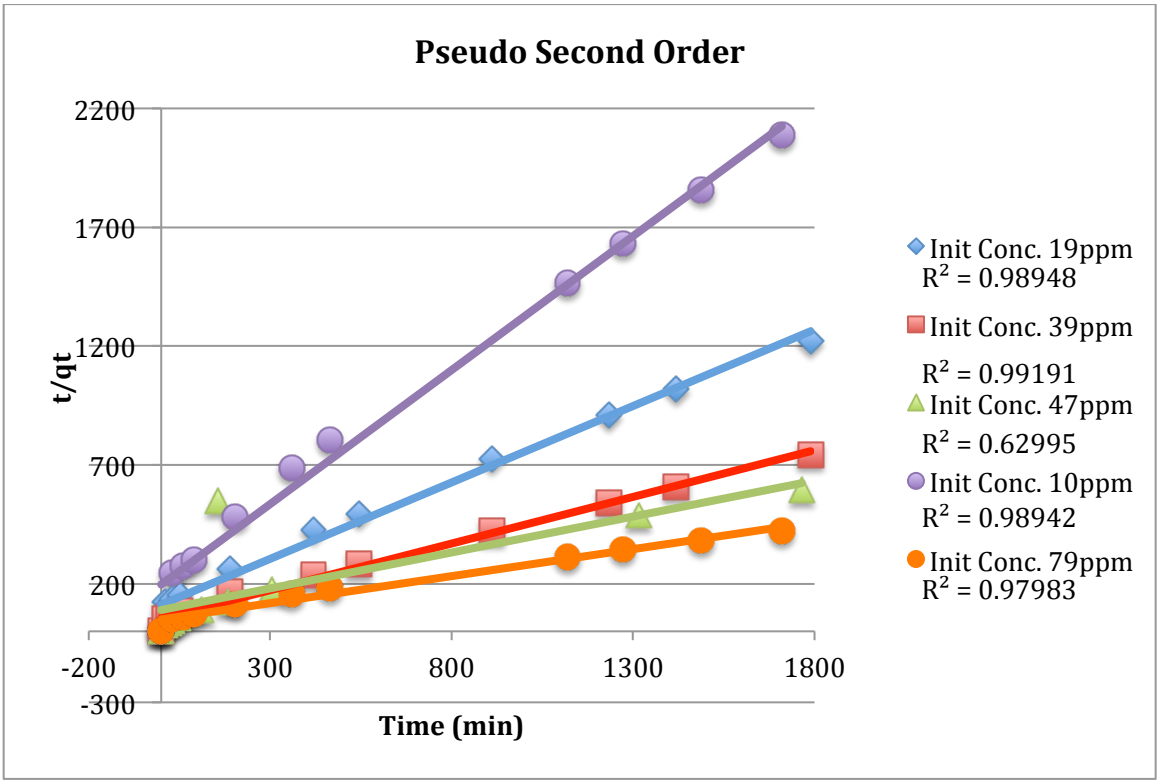

Figure 22. Pseudo Second-order plot for adsorption of fluoride on bone char

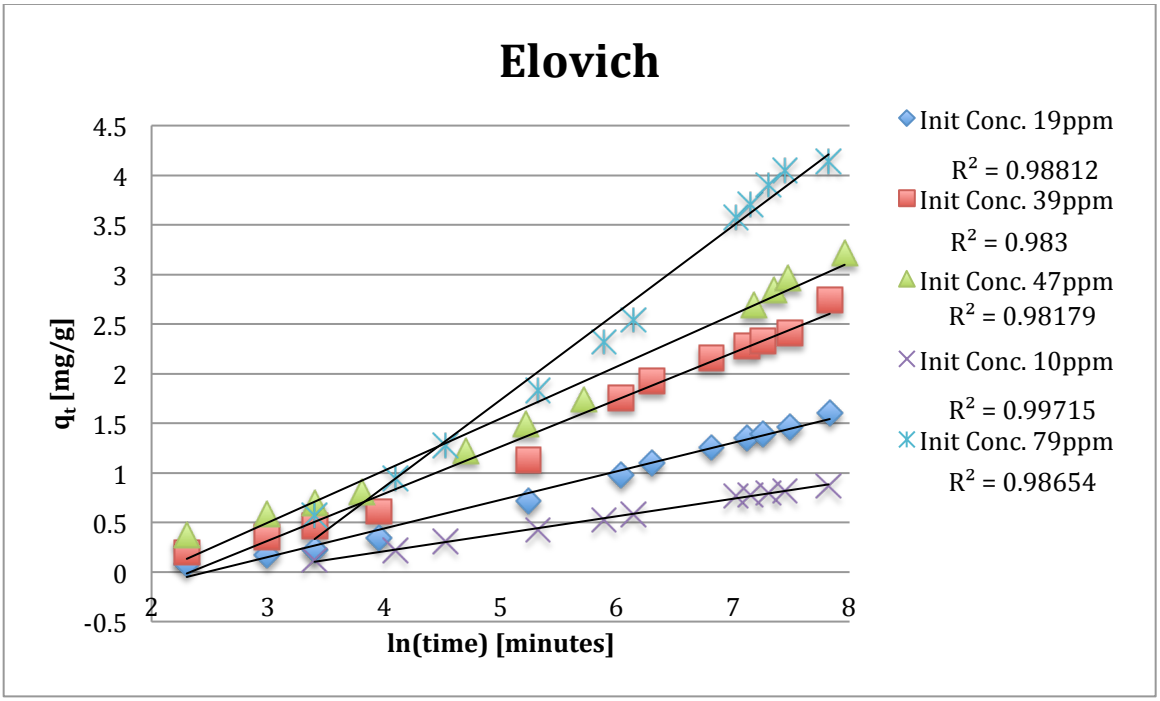

Figure 23. Elovich plot for adsorption of fluoride on bone char

The slopes of the best-fit lines in the Elovich model are equivalent to the $\frac{1}{\beta}$ term. As the initial concentration of fluoride increases the slope is shown to increase, subsequently decreasing β. Table 6 lists the constants (α and β) for the Elovich kinetics model for each of the initial concentrations tested.

Table 6. Constants for the Elovich model

Initial Concentration (ppm F^-)	Elovich, α	Elovich, β
10	0.011	5.666
19	0.024	3.473
39	0.046	2.111
47	0.068	1.908
79	0.045	1.140

The initial adsorption rate, α, and desorption constant, β, are shown to increase with increases in the initial fluoride concentration. This trend is in correlation with the increases in the adsorption capacity of the adsorbent. If fluoride is adsorbed at a faster rate and desorbed at a slower rate this allows for more fluoride to be retained resulting in a higher fluoride capacity correlating with higher solution concentrations. This trend supports basic adsorption theory and holds true for all concentrations and configurations tested.

CHAPTER 4

CONTACT PRECIPATATION METHOD

Introduction and Background

The addition of calcium and phosphate containing compounds to the influent fluoride-contaminated water will promote the removal of fluoride due to its precipitation as floroapatite and calcium fluoride [9], [12], [29], [30], [44]. This precipitation-mediated removal can act in addition to adsorption on bone char. To facilitate the use of this improved process with minimal user maintenance and input, the Catholic Dioceses of Nakuru, Kenya (CDN) has developed and begun production of a slow-release pellet that can be added to the bone char treatment tanks. The pellets are comprised of calcium-containing and phosphate-containing compounds as well as some fraction of finely ground bone char. The addition of these pellets to the bone char adsorption tanks is known as the contact precipitation (CP) process. Note that the abbreviation 'CP' refers to "Contact Precipitation" and not "Calcium Phosphate" because it is suspected that the pellets contain very little pure tricalcium phosphate due its low availability and high cost. It is more likely that the pellets contain a crude mixture of $Ca(OH)_2$, $CaHPO_4$, and $Ca(H_2PO_4)_2$, as well as other unidentified substituents.

Solubility Limited

The dissolution of the pellet is solubility limited and an excess of the solid pellets in a bone char adsorption system will result in relatively constant aqueous concentrations of Ca^{2+} and PO_4^{-3}. This constant concentration and the application of Le Chatelier's Principle will drive the precipitation of calcium fluoride until the concentration of fluoride is reduced to the point where the solubility product quotient, Q_{sp}, for the solution is less than the solubility product constant, K_{sp}, for CaF_2. The pure precipitation driven reaction is effective at removing fluoride from solution but is not effective at removing fluoride to low concentrations near the WHO's limit for drinking water of 1.5 ppm. To illustrate this principle, the chemical equilibrium modeler, Visual MINTEQ, was used to simulate the addition of increasing amounts of solid $Ca_3(PO_4)_2$ and $CaHPO_4$. Figure 24 shows that below the solubility point for the two salts, great increases in fluoride removal is achieved per small increase in the amount of compound added but then abruptly levels off at a fluoride concentration between 6 and 8 ppm F^- due to the equilibrium solubility constraints of CaF_2 and the calcium-phosphate salts.

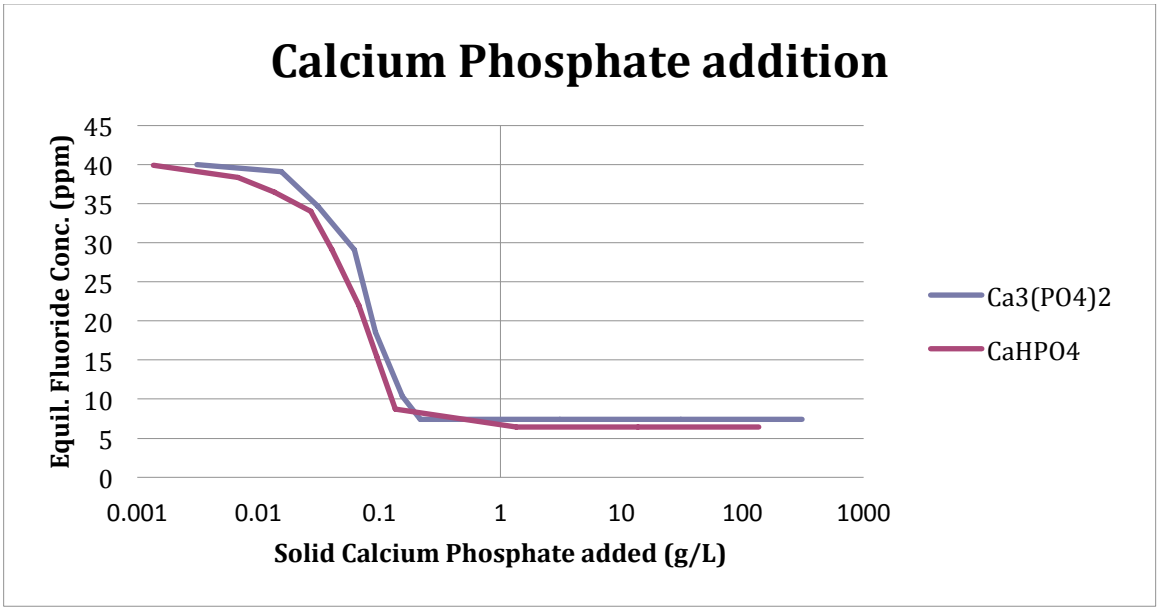

Figure 24. Equilibrium fluoride concentration for various concentrations of solid calcium phosphates added to solution.

To overcome this limitation, the precipitation process is coupled with bone char adsorption in the CP process to achieve higher levels of removal than either is capable of individually.

Bone Char to CP Pellet - Ratio Analysis

The interactions of bone char and CP pellets and the effects of those interactions on fluoride removal capacity if the CP process was a main focus of this study. Although theoretically the addition of pure calcium and phosphate components will lead to the precipitation of calcium fluoride, the kinetics of the precipitation are slow resulting in impractical contact times for the current applications [1]. The addition of bone char to the CP process has been shown to increase the rate of

reaction as well as the overall effectiveness of the system. To show the benefit of the mixed system over a system composed of just bone char or CP pellets alone, five different ratios of CP pellets to bone char were investigated while maintaining a constant total mass such that the sum of the masses of bone char and CP pellets was constant. Experimental results are shown in Figure 25.

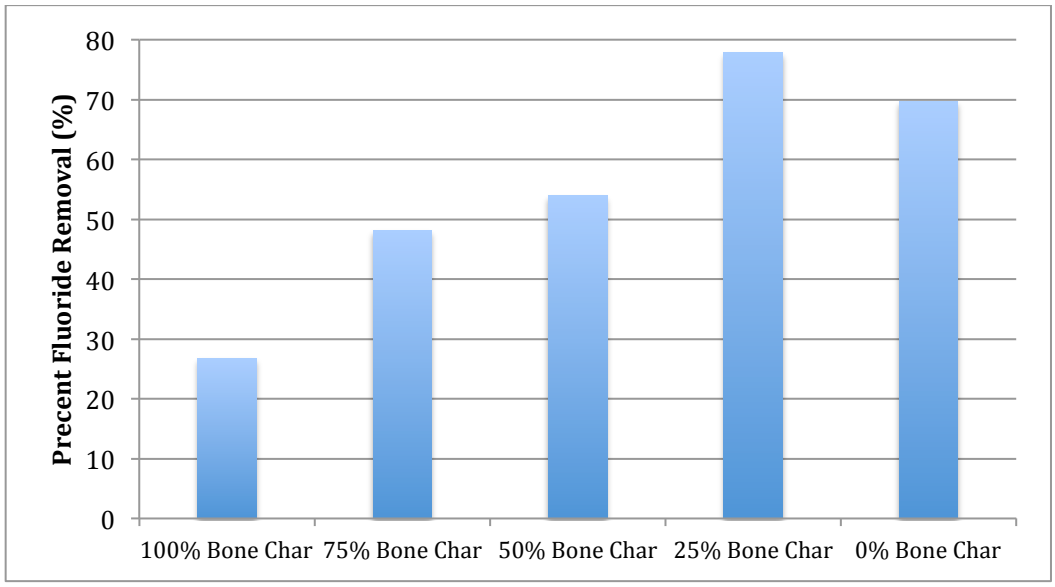

Figure 25. Influence of the bone char to CP pellet mass ratio on equilibrium fluoride removal efficiency. Initial fluoride concentration was 40 ppm and the total mass of bone char plus pellets was 2.0g.

Figure 25 indicates that a 1 to 3 mass ratio of bone char to CP pellets is the most efficient ratio tested for fluoride removal in a batch system. This ratio is congruent with the descriptions of the actual systems most commonly cited in the literature [1], [9]. The observation that a specific ratio of the two components can lead to

higher fluoride removals than either can individually points towards the bone char acting as a surface catalysis for the precipitation mechanism [30].

Solubility/Precipitation Analysis

The CP pellets manufactured at the Nakuru, Kenya facility contain an unknown portion of finely ground bone char and thus can facilitate the kinetically favored removal of fluoride on their own. Although bone char is present, removal using CP pellets alone is expected to be precipitation driven due to the abundance of calcium and phosphate salts in the pellets. Due to the low solubility of such salts the benefits to adding CP pellets at increasingly higher concentrations is expected to level off in a similar fashion to the trend seen with visual MINTEQ for the addition of solid $Ca_3(PO_4)_2$ and $CaHPO_4$ in Figure 24. The results of such an experimental study are presented in Figure 26 below.

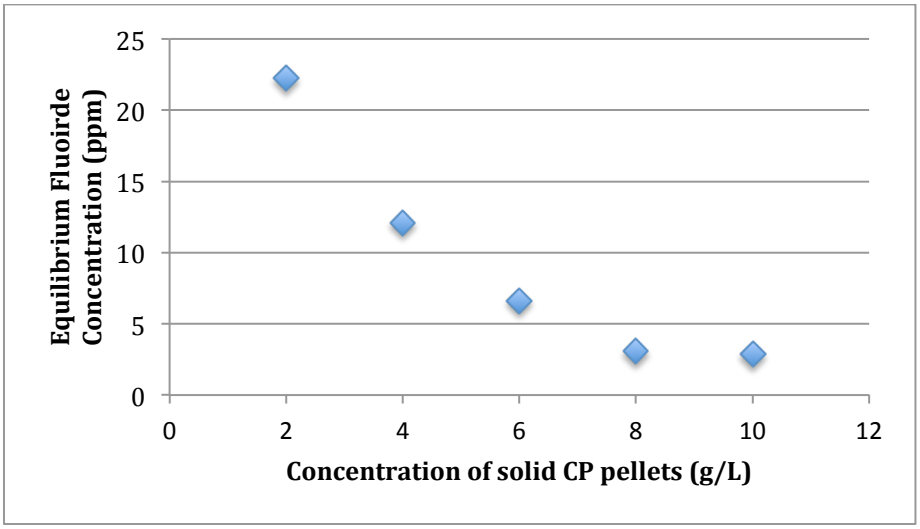

Figure 26. Equilibrium effects of CP pellets alone on fluoride concentration

Although similar in shape to that of the theoretical MINTEQ approximation, the CP pellet curve has several points of interest. The concentration of solid at which the equilibrium concentration of fluoride begins to level off is considerably higher (8g/L vs. 0.2g/L) than that of the MINTEQ prediction for the pure calcium phosphates. This confirms that the pellets are impure with a large portion of the mass not contributing soluble calcium and phosphate ions to the solution. The graph also levels out at a lower concentration of fluoride than predicted by the MINTEQ model for the pure salts. Several theories are postulated to explain why fluoride removals observed using the CP pellets exceed those theoretically predicted. For example, removal efficiency discrepancies between theoretical and laboratory results can be accounted for by the actual substituents of the pellet having a higher K_{sp} value than used in the MINTEQ simulation. A larger K_{sp} would result in more soluble salt and therefore a higher concentration of calcium and phosphate ions in solution. This higher concentration of ions would force more precipitation of fluoride as CaF_2 resulting in greater removal of fluoride. The greater than predicted fluoride removal capacity for the CP pellet study can also be accounted for by the available fraction of fine bone char that is known to be present in the CP pellets. The small bone char fraction (presumably less than 25 percent by mass) would increase the removal as demonstrated in Figure 25. Although understood individually, to completely

describe the CP method a better understanding of the coupling that exists between the adsorption and precipitation systems must be obtained.

Kinetics of Contact Precipitation

To describe the contact precipitation method, its effect on the kinetics of fluoride removal must be understood. Experimental results previously discussed, have confirmed, that the proportion of bone char in the CP pellet mixture dramatically affects the equilibrium adsorption capacity. Experimental data suggests a mass ratio of three parts CP pellets to one part bone char provides the best equilibrium fluoride removal. Although valuable, this information only provides insight to equilibrium conditions. The effect of the CP pellets on the kinetics of fluoride removal in the system is also an important factor in design. If the addition of the contact precipitant were to drastically slow down the rate of fluoride removal, the practicality of its use in the current removal systems would be diminished.

To analyze the effects of the CP method to the kinetics of the adsorption system the data for three experiments characterized by having similar initial and final concentrations of fluoride were evaluated; each trial had roughly equivalent initial and final concentrations of fluoride indicating that their overall removal was relatively the same. The removal mechanism for the individual experiments varied such that one DVR contained 2.0 g CP pellets, another with 5.0 g bone char, and one contained a mixture of 2.0 g bone char and 0.67 g CP pellets. Details of the three experiments are summarized in Table 7 below.

Table 7. Summary of three approximately equivalent-capacity trials

Removal Mechanism	Initial Fluoride Concentration, $[F^-]_i$	Equilibrium Fluoride Concentration, $[F^-]_e$	Change in Fluoride Concentration, $\Delta[F^-]$
2.0 g CP Pellets	38.6 ppm	10.7 ppm	27.9 ppm
5.0 g Bone Char	38.8 ppm	11.4 ppm	27.4 ppm
2.0 g Bone Char + 0.67 g CP Pellets	41.9 ppm	13.5 ppm	28.4 ppm

The small differences in the three selected configurations were normalized by plotting the data as a percent of fluoride removal versus time as seen in Figure 27.

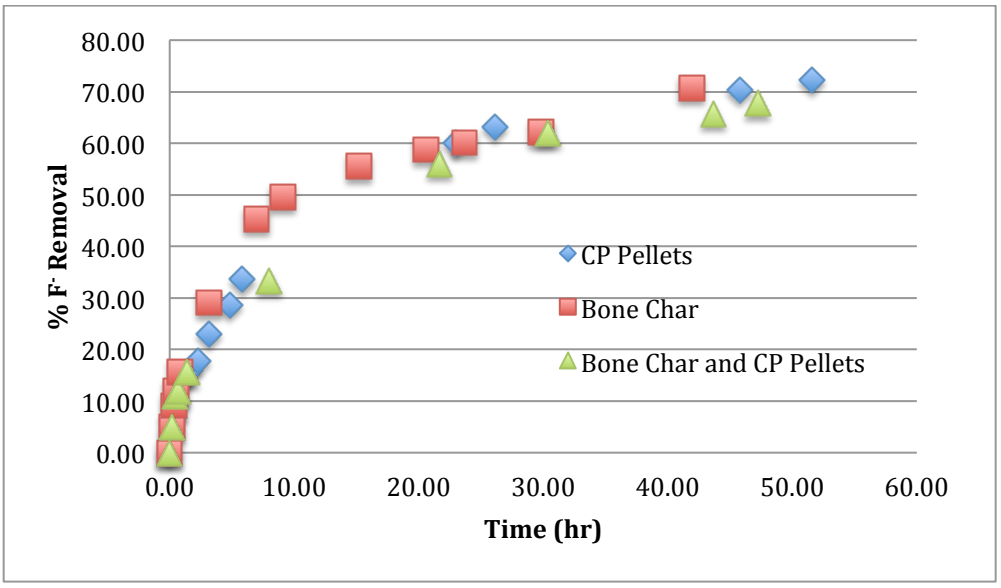

Figure 27. Percent of fluoride removal versus time.

Figure 27 shows that despite the differences in the composition of the adsorbent, removal kinetics remain relatively unaffected. The curve profile is logarithmic due

to the rate of removal slowing exponentially with time. This type of analysis was applied to a wide variety of trials with varying initial fluoride concentrations and masses of both CP pellets and bone char. Differing equilibrium capacities and concentrations were accounted for by normalizing the percent fluoride removal. In Figure 28, the y-axis represents the percent of the total possible removal under each set of experimental conditions.

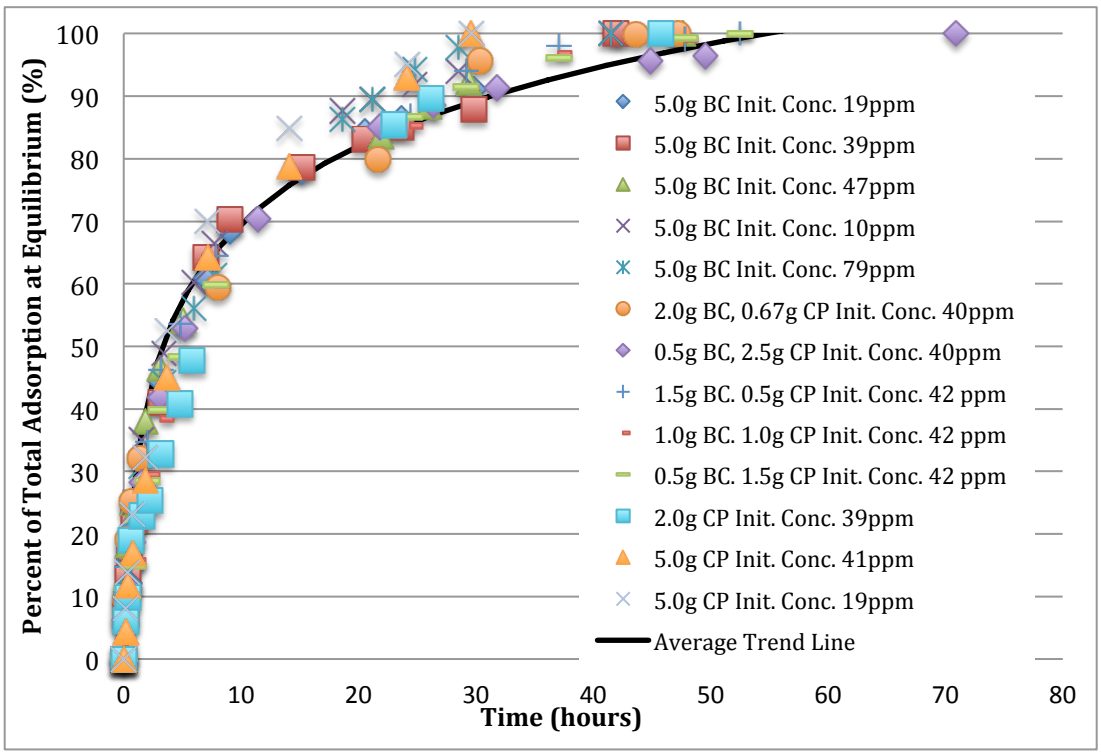

Figure 28. Percent of total possible fluoride removal with time.

Figure 28 demonstrates that the kinetics of removal displays a similar logarithmic trend for various initial conditions, amounts of adsorbent, and ratios of bone char (BC) to CP pellets until the 10-hour mark where approximately 70% of the possible

removal has occurred. After the 10-hour mark the data points begin to stray from the average path but continue with the general logarithmic trend. Although each of the trials presented in Figure 28 have differing capacities for fluoride removal, these data suggest that in a batch scenario at a given contact time any configuration will have removed an approximately equal percentage of the possible capacity for the specific configuration. Each data series was fit with a logarithmic model that fits the general form seen in Equation 19.

$$y = \boldsymbol{a}\boldsymbol{ln}(\boldsymbol{x}) + \boldsymbol{b} \qquad \textbf{Equation 19}$$

The coefficients a and b for all series were then averaged to determine the equation of the average trend line shown as Equation 20 and plotted on Figure 28. Coefficient 'a' was found to be 17.86 ± 1.44 (mean ± S.D.) and coefficient 'b' was found to be 28.53 ± 6.73.

$$\%\ of\ total\ capacity = 17.86 \ln(time) + 28.53 \qquad \textbf{Equation 20}$$

This information that the kinetics of the various configurations are similar, allows the design of fluoride adsorption vessels to be based primarily on maximizing the equilibrium capacity of the system without the need to account for changes in the kinetics or required contact time for removal.

CHPATER 5

CONCLUSIONS AND RECOMMENDATIONS

Conclusion

Bone charcoal is an effective adsorbent for the removal of fluoride from aqueous solutions. Equilibrium fluoride adsorption on bone char is best described by the Freundlich and Halsey adsorption isotherms (R^2 = 0.93 and 0.93, respectively), while bone char adsorption kinetics shows the highest correlation with the Elovich model, R^2 = 0.99. The addition of contact-precipitant pellets to bone char results in a greater removal of fluoride than either substituent is capable of individually. A mass ratio of one part bone char to three parts CP pellets was found to have a removal capacity approximately three times greater than that of bone char alone. The bone char was shown to act in a purely adsorptive manner in which the adsorptive capacity (2.7 mg F^- adsorbed/g bone char) was independent of the amount of bone char present. While the CP pellet response was indicative of a precipitation reaction, such that, after the solubility point was reached, further increases in the mass of CP pellets will result in no additional fluoride removal. The chemical and physical interactions between the CP pellets and bone char are largely not understood from a molecular standpoint. But, this study provides clarity of application for the end results of their interactions on fluoride removal.

The kinetics of bone char removal was studied with various initial fluoride concentrations, masses of adsorbents, and bone char to CP pellet mass ratios. The kinetics of all experiments were found to be similar such that after any given contact time, each system will have reached an equivalent percentage of their total possible removal. This indicates that the kinetics of fluoride removal is not dependent on the specific design parameters for each application. Although the parameters for removal kinetics should be incorporated into the design of a given system, they are independent of the parameters relating to the specific composition (BC:CP ratio) or location (groundwater fluoride concentration) of the adsorption tanks and thus design emphasis should be placed primarily on maximizing the equilibrium adsorption capacity and not on the kinetics of adsorption.

CHAPTER 6

RECOMMENDATIONS FOR FUTURE WORK

The work in this document presents a basic understanding for the adsorption of fluoride on bone charcoal in a batch system. All the data presented was collected using fluoride solutions prepared from deionized water. Future equilibrium and kinetic batch studies should be conducted with a stock solution that mimics the natural ion concentrations found in the groundwater of the Rift Valley. This analysis will allow for more appropriate predictions to be made regarding the capacity and kinetics of the system in the regions of their proposed application.

Future work should also incorporate the design and testing of fluoride adsorption in bone char columns under similar conditions to those observed in the Rift Valley. These trials should incorporate realistically scaled flow rates, periodic flow, and synthetic groundwater. Bench-scale experimental conditions should realistically represent the actual conditions experienced in Kenya and the surrounding regions such that results provide information about the expected life and breakthrough curve of the system.

Additional information is also needed to further understand the precipitation-based process that occurs with the addition of the Contact Precipitant (CP) pellets. The composition of the pellets as well as an understanding of the affects of various

calcium and phosphate containing compounds on fluoride removal should be studied. The data of these trials would then allow for a more complete understanding of the fluoride removal when bone char and CP pellets are used and could then allow for improvements to be made to the process.

REFERENCES

[1] J. Fawell, K. Bailey, J. Chilton, E. Dahi, L. Fewtrell, and Y. Magara, "Fluoride in Drinking-water," IWA Publishing, Dec. 2006.

[2] W. D. Alessandro, "Human fluorosis related to volcanic activity : a review," *Environmental Toxicology Transaction: Biomedicine and Health*, vol. 10, pp. 21-30, 2006.

[3] UNICEF, "NoFluoride.com." [Online]. Available: http://www.nofluoride.com/Unicef_fluor.cfm. [Accessed: 17-Jan-2012].

[4] D. Hem, *Study and Interpretation the Chemical of Natural of Characteristics Water*, 3rd ed. 1985.

[5] "Water Resource Quality Nalgonda Technique," *eawag aquatic research*. [Online]. Available: http://www.eawag.ch/forschung/qp/wrq/mitigation_framework/technologies/fluoride_removal/nalgonda/index_EN. [Accessed: 17-Jan-2012].

[6] E. Dahi, F. Mtalo, B. Njau, and H. Bregnhj, "Defluoridation using the Nalgonda Technique in Tanzania The Nalgonda technique," in *22nd WEDC Conference*, 1996, pp. 266-268.

[7] E. Dahi, "Contact precipitation for defluoridation of water," in *22nd WEDC Conference : Discussion paper*, 1996, pp. 262-265.

[8] H. Korir et al., "The development of bone char-based filters for the removal of fluoride from drinkning water," in *34th WEDC Interbational Confrence*, 2009.

[9] H. Albertus, J. Bregnhøj, and M. Kongpun, "Bone Char Quality and Defluoridation Capacity in Contact Precipitation," in *3rd International Workshop on Fluorosis Prevention and Defluoridation of Water*, 2000, pp. 61-72.

[10] K. Muller and P. Jacobsen, "CDN's Experiences in Producing Bone Char," 2007.

[11] J. A. H. Bregnhøj and M. Kongpun, "Bone Char Quality and Defluoridation Capacity in Contact Precipitation," pp. 61-72.

[12] E. Dahi, "Development of the Contact Precipitation Method for Appropriate Defluoridation of Water," in *2nd International Workshop on Fluoride Prevention and Deflouridation of Water*, 1997, pp. 128-137.

[13] H. Freundlich, "Ueber die Adsorption in Loesungen," *Zeitschrift fr Physikalische Chemie*, vol. 57, pp. 385-470, 1907.

[14] M. S. Onyango, Y. Kojima, O. Aoyi, E. C. Bernardo, and H. Matsuda, "Adsorption equilibrium modeling and solution chemistry dependence of fluoride removal from water by trivalent-cation-exchanged zeolite F-9.," *Journal of colloid and interface science*, vol. 279, no. 2, pp. 341-50, Nov. 2004.

[15] I. Langmuir, "The Adsorption of Gases on Plane Surfaces of Glass, Mica, and Platinum," *Journal of the American Chemical Society*, vol. 40, no. 9, pp. 1361-1403, 1918.

[16] Z. V. P. Murthy, T. Prabhakar, and R. Kumar, "Isotherm and Kinetics Modeling of Fluoride Removal from Industrial Effluent by Alumina," *Chemical Product and Process Modeling*, vol. 5, no. 1, Sep. 2010.

[17] K. R. Hall, L. C. Eagleton, A. Acrivos, and T. Vermeulen, "Pore- and Solid-Diffusion Kinetics In Fixed-Bed Adsorption Under Constant-Pattern Conditions," *Industrial and Engineering Chemistry Fundamentals*, vol. 5, no. 2, pp. 212-223, 1966.

[18] "Adsorption Principles," *Lecture Notes: San Jose State Univeristy*, 2011. [Online]. Available: www.engr.sjsu.edu. [Accessed: 26-Feb-2012].

[19] N. A. Oladoja, C. O. Aboluwoye, and Y. B. Oladimeji, "Kinetics and Isotherm Studies on Methylene Blue Adsorption onto Ground Palm Kernel Coat," *Turkish Journal of Engineering and Environmental Sciences*, vol. 32, pp. 303-312, 2008.

[20] M. J. Temkin and V. Pyzhev, "Recent Modifications to Langmuir Isotherms," *Acta Physiochim URSS*, vol. 12, pp. 217-222, 1940.

[21] E. Khosla, S. Kaur, and P. N. Dave, "Surfactant modified tea waste as a novel adsorbent for the removal of Basic dye," *Der Chemica Sinica*, vol. 2, no. 5, pp. 87-102, 2011.

[22] B. K. Suyamboo, "Equilibrium, Thermodynamic and Kinetic Studies on Adsorption of a Basic Dye by Citrullus Lanatus Rind," *Iranica Journal of Energy & Environment*, vol. 3, no. 1, pp. 23-34, 2012.

[23] N. a. Oladoja, I. a. Ololade, J. a. Idiaghe, and E. E. Egbon, "Equilibrium isotherm analysis of the sorption of congo red by palm kernel coat," *Central European Journal of Chemistry*, vol. 7, no. 4, pp. 760-768, Oct. 2009.

[24] I. Abe, S. Iwasaki, T. Tokimoto, N. Kawasaki, T. Nakamura, and S. Tanada, "Adsorption of fluoride ions onto carbonaceous materials.," *Journal of colloid and interface science*, vol. 275, no. 1, pp. 35-9, Jul. 2004.

[25] N. A. Medellin-castillo et al., "Adsorption of Fluoride from Water Solution on Bone Char," *Industrial and Engineering Chemical Research*, vol. 46, pp. 9205-9212, 2007.

[26] R. Leyva-Ramos, J. Rivera-Utrilla, N. a. Medellin-Castillo, and M. Sanchez-Polo, "Kinetic modeling of fluoride adsorption from aqueous solution onto bone char," *Chemical Engineering Journal*, vol. 158, no. 3, pp. 458-467, Apr. 2010.

[27] W. Li, C.-Y. Cao, L.-Y. Wu, M.-F. Ge, and W.-G. Song, "Superb fluoride and arsenic removal performance of highly ordered mesoporous aluminas.," *Journal of hazardous materials*, vol. 198, pp. 143-50, Dec. 2011.

[28] E. Tchomgui-Kamga, E. Ngameni, and a Darchen, "Evaluation of removal efficiency of fluoride from aqueous solution using new charcoals that contain calcium compounds.," *Journal of colloid and interface science*, vol. 346, no. 2, pp. 494-9, Jun. 2010.

[29] C. S. Sundaram, N. Viswanathan, and S. Meenakshi, "Defluoridation chemistry of synthetic hydroxyapatite at nano scale: equilibrium and kinetic studies.," *Journal of hazardous materials*, vol. 155, no. 1-2, pp. 206-15, Jun. 2008.

[30] S. Gao, R. Sun, Z. Wei, H. Zhao, H. Li, and F. Hu, "Size-dependent defluoridation properties of synthetic hydroxyapatite," *Journal of Fluorine Chemistry*, vol. 130, no. 6, pp. 550-556, Jun. 2009.

[31] S. Lagergren, "About the theory of so-called adsorption of soluble substances," *Kungliga Svenska Vetenskapsakademiens. Handlingar*, vol. 24, no. 4, p. 1898, 1898.

[32] N. Renugadevi, R. Sangeetha, and P. Lalitha, "Kinetics of the adsorption of methylene blue from an industrial dyeing effluent onto activated carbon prepared from the fruits of Mimusops Elengi," *Archives of Applied Science Research*, vol. 3, no. 3, pp. 492-498, 2011.

[33] C.-ryul Lee, H.-seon Kim, I.-hyuk Jang, J.-hyeok Im, and N.-gyu Park, "Pseudo First-Order Adsorption Kinetics of N719 Dye on TiO2 Surface," *ACS Applied Materials and Interfaces*, vol. 3, pp. 1953-1957, 2011.

[34] S.-an Ong, C.-eng Seng, and P.-eng Lim, "KINETICS OF ADSORPTION OF CU (II) AND CD (II) FROM AQUEOUS," *Electronic Journal of Environmental, Agricultural, and Food Chemistry*, vol. 6, no. 2, pp. 1764-1774, 2007.

[35] G. Alagumuthu and M. Rajan, "Kinetic and equilibrium studies on fluoride removal by zirconium (IV): Impregnated groundnut shell carbon," *Hemijska industrija*, vol. 64, no. 4, pp. 295-304, 2010.

[36] Y. S. Ho, "Adsorption of heavy metals from waste streams by peat," The University of Birmingham, Birmingham, U.K., 1995.

[37] G. Tamman and K. W., "Chemical Reviews, 60(3):267-312.," *Z. Anorg. Chem.*, pp. 123-196, 1922.

[38] S. Elovich, "Chemical Reviews, 60(3):267-312.," in *New York*, 1959, vol. 11, no. 1939, p. 253.

[39] Y. Zeldovich, "Chemical Reviews, 60(3):267-312.," *Acta Physicochim*, vol. 1, p. 449, 1934.

[40] S. Elovich and G. M. Zhabrova, "G. M. Zhur. Fiz. Khim.," *G. M. Zhur. Fiz. Khim.*, vol. 13, pp. 1761-1775, 1939.

[41] R.-S. Juang, S.-H. Lin, and C.-H. Cheng, "Liquid-phase adsorption and desorption of phenol onto activated carbons with ultrasound.," *Ultrasonics sonochemistry*, vol. 13, no. 3, pp. 251-60, Apr. 2006.

[42] R.-shin Juang and M.-lian Chen, "Application of the Elovich Equation to the Kinetics of Metal Sorption with Solvent-Impregnated Resins," *Indstrial and Engineering Chemical Research*, vol. 36, pp. 813-820, 1997.

[43] C. W. Cheung, J. F. Porter, and G. Mckay, “Sorption kinetic analysis for the removal of cadmium ions from effluents using bone char.,” *Water research*, vol. 35, no. 3, pp. 605-12, Mar. 2001.

[44] A. Bhatnagar, E. Kumar, and M. Sillanpää, “Fluoride removal from water by adsorption—A review,” *Chemical Engineering Journal*, vol. 171, no. 3, pp. 811-840, Jul. 2011.

APPENDIX 1

BONE CHAR ADSORPTION DATA

10/31/11	10 g Coarse Bone Char With Spout (Red) ppm	500mL Solution No Spout (Green)ppm
4:10:00 PM	9.71	28.96
4:40:00 PM	7.08	23.96
5:18:00 PM	5.65	18.54
6:15:00 PM	4.09	14.57
7:00:00 PM	3.27	12.06
8:24:00 PM	2.62	10.71
10:45:00 PM	1.7	8.55
12:53:00 AM	1.35	6.94
8:55:00 AM	0.66	4.44
11:00:00 AM	0.53	3.85
4:10:00 PM	0.37	3.03
9:30:00 PM	0.25	2.42
8:50:00 AM	0.24	1.91
1:41:00 PM	0.21	1.47

11/2/11	5 g CoarseBone Char With Spout (Red) ppm	500mL Solution No Spout (Green)ppm
3:56:00 PM	18.79	38.78
4:06:00 PM	17.99	36.82
4:16:00 PM	17.08	35.24
4:26:00 PM	16.55	34.18
4:48:00 PM	15.4	32.7
7:05:00 PM	11.66	27.5
10:55:00 PM	9.01	21.17
1:00:00 AM	7.79	19.52
7:08:00 AM	6.25	17.22
12:30:00 PM	5.24	15.97
3:35:00 PM	4.9	15.47
9:45:00 PM	4.15	14.68
9:50:00 AM	2.72	11.36

11/4/11	5 g CoarseBone Char With Spout (Red) ppm	500mL Solution No Spout (Green)ppm
1:30:00 PM	0.05	47.05
1:40:00 PM	-	43.24
1:50:00 PM	-	41.21
2:00:00 PM	-	40.07
2:15:00 PM	-	38.95
3:20:00 PM	0.09	34.81
4:35:00 PM	-	32.12
6:35:00 PM	-	29.64
11:25:00 AM	0.07	20.13
3:30:00 PM	-	18.6
6:55:00 PM	-	17.4
1:08:00 PM	-	14.87

11/9/11	5 g CoarseBone Char With Spout (Red) ppm	500mL Solution No Spout (Green)ppm
3:00:00 PM	9.78	79.22
3:30:00 PM	8.55	73.5
4:00:00 PM	7.6	69.74
4:32:00 PM	6.73	66.49
6:25:00 PM	5.52	60.91
9:00:00 PM	4.53	56.03
10:46:00 PM	3.99	53.84
9:40:00 AM	2.14	43.52
12:13:00 PM	1.98	42.17
3:47:00 PM	1.78	40.22
7:30:00 PM	1.59	38.76
8:30:00 AM	1.07	37.85

11/14/11	5 g Medium Bone Char With Spout (Red) ppm	500mL Solution No Spout (Green)ppm
12:56:00 PM	9.35	27.13
1:08:00 PM	8.41	24.39
1:21:00 PM	6.96	21.92
1:37:00 PM	6.25	20.91
1:58:00 PM	5.71	19.67
3:15:00 PM	4.37	15.86
5:20:00 PM	3.1	12.97
7:56:00 PM	2.42	11.43
1:24:00 AM	1.61	8.86
9:30:00 AM	1.03	7.7
12:22:00 PM	0.78	7.15
3:58:00 PM	0.66	6.69

11/16/11	5 g Medium Bone Char With Spout (Red) ppm	500mL Solution No Spout (Green)ppm
1:23:00 PM	17.76	37.12
1:34:00 PM	16.1	33.78
1:44:00 PM	14.94	31.73
1:55:00 PM	13.93	29.8
2:39:00 PM	11.86	27.23
4:15:00 PM	9.29	22.82
5:56:00 PM	7.64	19.36
9:43:00 PM	6.16	13.88
9:23:00 AM	3.42	12.26
4:50:00 PM	2.93	11.27
7:25:00 PM	2.59	10.95

11/20/11	5 g Medium Bone Char With Spout (Red) ppm	500mL Solution No Spout (Green)ppm
2:01:00 PM	57.2	43.7
2:11:00 PM	54.4	41.2
2:21:00 PM	51.9	37.7
2:33:00 PM	48.95	36.27
2:48:00 PM	46.36	34.21
3:14:00 PM	44.59	32.27
4:17:00 PM	37.27	27.08
5:54:00 PM	33.42	23.08
10:35:00 PM	32.64	21.96
9:15:00 PM	27.31	15.43
8:46:00 AM	25.51	13.6

11/27/11	2 g Coarse BC + 6g CP With Spout (Red) ppm	500mL Solution No Spout (Green)ppm
10:55:00 AM	31.76	11.14
11:06:00 AM	29.7	9.54
11:18:00 AM	26.5	8.29
11:28:00 AM	23.73	7.22
11:50:00 AM	20.03	5.95
12:31:00 PM	16.26	4.22
1:19:00 PM	13.35	3.1
9:39:00 PM	3.18	0.5
11:38:00 PM	2.46	0.32
1:35:00 PM	1.11	0.22
11:08:00 PM	0.59	0.08

11/30/11	5g CP	500mL Solution
	With Spout (Red) ppm	No Spout (Green)ppm
8:24:00 AM	40.56	18.57
8:34:00 AM	38.99	17.15
8:44:00 AM	36.32	16.11
8:54:00 AM	34.5	14.48
9:19:00 AM	30.28	12.86
10:25:00 AM	24.38	9.27
12:18:00 PM	17.5	6.17
3:44:00 PM	12.27	3.53
10:40:00 PM	7.15	1.71
8:44:00 AM	4.64	0.85
2:10:00 PM	3.47	0.57

12/3/11	2g BC and CP either .67g or .2g	500mL Solution
	With Spout (Red) ppm	No Spout (Green)ppm
	BC:CP 10:1	BC:CP 3:1
1:45:00 PM	40.11	41.89
1:55:00 PM	38.41	39.8
2:08:00 PM	36.63	37.36
2:23:00 PM	35.5	36.92
3:06:00 PM	34.26	35.36
9:45:00 PM	29.26	27.91
11:25:00 AM	25.53	21.86
8:08:00 PM	22.65	15.89
9:25:00 AM	21.89	14.34
12:57:00 PM	21.86	13.54

12/8/11	2g BC and CP either 0.1g or 1.0g	500mL Solution
	With Spout (Red) ppm	No Spout (Green)ppm
	BC:CP 20:1	BC:CP 2:1
9:27:00 AM	38.82	39.91
9:40:00 AM	38.21	37.46
10:58:00 AM	36.3	34.48
11:40:00 AM	35.84	32.5
2:48:00 PM	32.78	26.78
3:48:00 PM	31.86	25.75
10:50:00 PM	29.21	20.56
12:35:00 PM	26.37	15
5:55:00 PM	25.05	13.9
12:45:00 PM	24.71	10.97
9:05:00 PM	23.18	9.88
1:45:00 PM	22.63	8.64
2:30:00 PM	21.82	7.35

12/12/11	2g BC and CP either 2.0g or 0.4g With Spout (Red) ppm BC:CP 1:1	500mL Solution No Spout (Green)ppm BC:CP 5:1
7:41:00 PM	38.27	38.11
7:52:00 PM	34.79	36.78
8:08:00 PM	33.04	36.78
8:21:00 PM	31.75	35.78
8:48:00 PM	30.03	34.51
9:36:00 PM	27.3	32.91
10:18:00 PM	24.24	31
11:12:00 PM	23.02	31
9:15:00 AM	13.68	25.41
2:08:00 PM	10.8	23.39
8:15:00 PM	9.29	22.05
9:08:00 AM	7.11	20.6
7:13:00 PM	5.9	18.83
10:30:00 AM	4.69	16.96
4:28:00 PM	4.32	16.49
6:28:00 PM	4.16	16.67
10:38:00 AM	3.94	15.72

12/17/11	2.0g BC 2.0g CP With Spout (Red) ppm CP only	500mL Solution No Spout (Green)ppm BC only
1:51:00 PM	38.6	37.14
2:02:00 PM	36.95	36.95
2:12:00 PM	35.93	37.54
2:28:00 PM	33.45	35.79
3:27:00 PM	32.4	35.36
4:04:00 PM	31.73	36.85
5:00:00 PM	29.71	35.27
6:40:00 PM	27.54	34.85
7:40:00 PM	25.64	34.3
12:50:00 PM	15.43	29.41
4:00:00 PM	14.25	27.37
11:37:00 AM	11.46	26.32
5:27:00 PM	10.7	26.44

1/4/12	0.5 g BC:1 g CP	0.5 g BC:1.5 g CP	0.5 g BC:2.5 g CP	0.5 g BC:5 g CP
500mL Soln.	**A**	**B**	**C**	**D**
	1 to 2	**1 to 3**	**1 to 5**	**1 to 10**
12:17:00 PM	40.21	40.21	40.21	40.21
12:24:00 PM	39.43	38.82	37.91	36.17
12:35:00 PM	38.51	37.62	36.74	34.37
12:47:00 PM	38.51	37.03	36.03	32.54
1:07:00 PM	37.47	36.03	33.31	28.47
1:47:00 PM	36.02	33.97	29.73	23.68
3:24:00 PM	33.31	30.44	24.73	16.64
5:30:00 PM	30.8	27.59	20.64	12.25
11:44:00 PM	27.42	22.42	14.17	6.39
10:05:00 AM	21.97	16.21	8.71	2.83
2:41:00 PM	19.88	14.78	7.42	2.06
8:05:00 PM	19.2	13.66	6.41	1.64
9:10:00 AM	17.27	11.47	4.8	1.06
1:50:00 PM	16.86	11.24	4.51	0.99
11:10:00 AM	14.65	9.09	3.19	0.65

1/4/12	1.0g BC:1.0 g CP	0 g BC:4.0 g CP	1.5 g BC:0.5 g CP
500mL Soln.	**A**	**B**	**C**
2:48:00 PM	40.09	40.09	40.09
3:19:00 PM	37.78	35.75	37.63
4:30:00 PM	35.61	30.29	35.33
7:17:00 PM	31.51	22	32.26
10:53:00 AM	23.57	8.58	25.73
8:45:00 PM	22.03	6.29	24.39
10:50:00 AM	19.82	4.07	22.37
6:45:00 PM	18.47	3.17	20.85

	Medium Bone Char			
1/10/12	2.0g BC:0 g CP	1.5 g BC:0.5 g CP	1.0 g BC:1.0 g CP	0.5 g BC:1.5 g CP
500mL Soln.	**A**	**B**	**C**	**D**
9:50:00 AM	42.24	42.24	42.24	42.24
10:08:00 AM	39.98	39.2	39.51	38.74
10:40:00 AM	37.55	37.84	38.29	37.69
11:51:00 AM	34.58	35.12	34.85	33.51
1:00:00 PM	33.12	32.73	32.6	30.02
2:41:00 PM	32.22	31.22	30.38	27.43
5:42:00 PM	30.74	28.98	27.21	23.91
10:15:00 AM	30.65	24.39	20.83	15.68
3:00:00 PM	29.7	22.89	19.25	14.21
10:55:00 PM	29.3	22.08	17.93	12.79
9:40:00 AM	29.85	21.86	17.32	11.81
2:20:00 PM	30.21	21.68	17.11	11.62

	Coarse Bone Char			
1/13/12	1.0g BC:4.0 g CP	1.0 g BC:2.0 g CP	0 g BC:1.0 g CP	0 g BC:3.0 g CP
500mL Soln.	**A**	**B**	**C**	**D**
10:00:00 AM	38.72	38.72	38.72	38.72
10:40:00 AM	35.61	36.03	38.12	35.32
11:28:00 AM	31.2	34.35	37.06	31.96
12:32:00 PM	27.24	31.58	36.03	30.34
2:17:00 PM	23.68	29.15	35.32	26.27
5:35:00 PM	18.41	24.45	32.61	21.17
8:37:00 PM	14.65	20.23	29.96	17.22
10:17:00 AM	9.65	13.49	25.15	10.1
6:00:00 PM	8.33	11.53	23.84	8.26
12:10:00 PM	6.87	8.53	20.97	5.36

APPENDIX 2

CHARACTERIZATION OF BONE CHAR FRACTIONS

Coarse Bone Char	Original Mass (g)	Final Mass (g)	Difference in Mass (g)	% Composition by mass
Top	53.30	53.30	0.00	0.00
#6	166.41	233.72	67.31	29.80
#20	154.06	310.69	156.63	69.35
#40	155.28	155.98	0.70	0.31
#60	150.87	151.19	0.32	0.14
#100	144.63	144.93	0.30	0.13
#230	138.18	138.54	0.36	0.16
Bottom	122.54	122.77	0.23	0.10
		Total:	225.85	100.00
Bulk Packing Density	909.64	g/L		

Medium Bone Char	Original Mass (g)	Final Mass (g)	Difference in Mass (g)	% Composition by mass
Top	53.30	53.30	0.00	0.00
#6	166.42	166.71	0.29	0.11
#20	153.97	402.53	248.56	96.30
#40	155.19	162.48	7.29	2.82
#60	150.88	151.58	0.70	0.27
#100	144.60	145.13	0.53	0.21
#230	138.20	138.72	0.52	0.20
Bottom	122.56	122.78	0.22	0.09
		Total:	258.11	100.00
Bulk Packing Density	918.8	g/L		

Fine Bone Char	Original Mass (g)	Final Mass (g)	Difference in Mass (g)	% Composition by mass
Top	53.30	53.30	0.00	0.00
#6	166.41	166.45	0.04	0.02
#20	153.96	221.29	67.33	36.31
#40	155.19	266.12	110.93	59.83
#60	150.89	154.92	4.03	2.17
#100	144.61	146.13	1.52	0.82
#230	138.19	139.33	1.14	0.61
Bottom	122.55	122.98	0.43	0.23
		Total:	185.42	100.00
Bulk Packing Density	908.12	g/L		

APPENDIX 3

BONE CHAR PHOTOS

Coarse Bone Char

Medium Bone Char

Fine Bone Char

APPENDIX 4

KENYAN WATER QUAILITY REPORT

* MAJI NI UHAI * WATER IS LIFE *

WATER QUALITY

Catholic Diocese of Nakuru Water Programme

P.O. Box 938
Nakuru
KENYA

Tel.: +254 - 51 - 2216 264/5
Mob: +254 - 0722 867 551

Telefax: + 254 - 51 - 2214 151
E-Mail:cdnwaterquality@yahoo.com

When replying please quote our Ref. No.

Test type: *Standard Chemical Water Analysis*

Our ref.: *091103NWG T712*

Submitted by: *Samuel P.Harrell*

Date received: *06-11-09*

Source: *Borehole*

Date taken: *?*

Conclusions:

The water is slighty turbid, with colour.
The water is soft, with very high alkalinity.
The Fluoride content exceeds the maximum value of 1.5 mg/l, thus making the water is not suitable for cooking and drinking.Defluoridation is recommended.
The Iron content exceeds the Guideline Value of 0.3 mg/l and this may give staining problems in laundry etc.
The Alkalinity, Sulfate and Sodium contents exceeds the Guideline Value of 500 mg/l, 250 mg/l and 200 mg/l respectively and this is likely to give the water an unpleasant taste.
The water is oversaturated with respect to Calcium Cabornate and this may enhance scale deposition.
Based on the measured parameters the water can be used for other domestic purposes.
The water is not suitable for irrigation.

General Remarks:

The conclusions and recommendations follows World Health Organization (WHO) guidelines (1994). The conclusions are based only of the parameters measured.
Shallow wells, springs, surface water: *The chemical components of the water is likely to change during a season.*
Deep wells: *The chemical components of the water is likely to change in the first period after drilling the borehole, it is therefore recommended to retest the water after e.g. 6 months.*
Test Methods: *the test methods follows the "Standard Methods for the examination of Water and Wastewater" published by American Public Health Association and American Water Works Association.*
Further information *on the individual test is available in the folder "Interpretation of Water Test Results" from CDN Water Quality.*

CDN Water Quality Laboratory — *12-Nov-09* *Date*

CDN WATER LABORATORY
Tel.: 051 - 2216264/5
FAX: 051 - 2214151
12 NOV 2009
Email: cdnwaterlaboratory@yahoo.com
P.O. Box 938, NAKURU, KENYA

MAJI NI UHAI * WATER IS LIFE *

WATER QUALITY

Catholic Diocese of Nakuru Water Programme

P.O. Box 938
Nakuru
KENYA

Tel.: +254 - 51 - 2216 264/5
Mob: +254 - 0722 867 551

Telefax: + 254 - 51 - 2214 151
E-Mail:cdnwaterquality@yahoo.com

When replying please quote our Ref. No.

Our ref.: *091103NWG*

Test type: *Standard Chemical Water Analysis* *T712*

Submitted by: *Samuel P.Harrell* Date received: *06-11-09*

Source: *Borehole* Date taken: *?*

Physical and Aggregate Properties:	***Results***	***Units***
Temperature		°C
Colour (true)	*40*	Colour units/l
pH	*7.9*	
Turbidity	*5*	NTU
Conductivity	*250*	mS/m
Acidity (pH=8.3)	*32*	mg $CaCO_3$/l
Acidity (pH=10.8)	*1395*	mg CaCO3/l
Alkalinity (phenolpthhalein)	*0*	mg $CaCO_3$/l
Alkalinity total (pH=4.5)	*1331*	mg $CaCO_3$/l
Hardness total	*32*	mg $CaCO_3$/l
Total solids (residue dried at 110C)	*2180*	mg/l
Total dissolved solids (residue dried at 180C)	*1994*	mg/l
Settleable solids	*Less than 0.1*	ml/l
SAR (Sodium Absorption Ratio)	*20.1*	-
RSC (Residual Sodium Carbonate)	*26.2*	meq/l
SI (Saturation index)	*0.7*	
Metals:		
Calcium (Ca^{++})	*10*	mg/l
Iron (Fe^{+++})	*0.8*	mg/l
Magnesium (Mg^{++})	*2*	mg/l
Manganese (Mn^{++})	*Less than 0.1*	mg/l
Sodium (Na^{+})	*524*	mg/l
Inorganic Nonmetallic constituents:		
Carbon dioxide (CO_2)	*32.5*	mg/l
Bicarbonate (HCO_3^-)	*1611*	mg/l
Carbonate (CO_3^{--})	*6.0*	mg/l
Chlorine (Cl)	*Less than 0.05*	mg/l
Nitrate + Nitrite (NO_3^--N)	*3*	mg/l
Total Reactive Phosphorous (P)	*1*	mg/l
Chloride (Cl^-)	*49*	mg/l
Fluoride (F^-)	*21.3*	mg/l
Silica (SiO_2)	*35*	mg/l
Sulfate (SO_4^{--})	*258*	mg/l

CDN WATER LABORATORY
TEL: 051 - 2215264/5
FAX: 051 - 2214151
12 NOV 2009
Email: cdnwaterlaboratory@yahoo.com
P.O. Box 938, NAKURU, KENYA

WATER QUALITY

Catholic Diocese of Nakuru Water Programme

P.O. Box 938
Nakuru
KENYA

Tel.: +254 - 51 - 2216 264/5
Mob: +254 - 0722 867 551

Telefax: + 254 - 51 - 2214 151
E-Mail:cdnwaterquality@yahoo.com

When replying please quote our Ref. No.

Our ref.: *091103NWG*
T712

Test type: *Standard Chemical Water Analysis*

Submitted by: *Samuel P.Harrell*

Date received: *06-11-09*

Source: *Filtered*

Date taken: *?*

Conclusions:

The water is clear, but with slight colour.
The water is very soft, with very high alkalinity.
The Fluoride content exceeds the maximum value of 1.5 mg/l, thus making the water is not suitable for cooking and drinking.Defluoridation is recommended.
The Alkalinity, Sulfate and Sodium contents exceeds the Guideline Value of 500 mg/l, 250 mg/l and 200 mg/l respectively and this is likely to give the water an unpleasant taste.
The water is oversaturated with respect to Calcium Cabornate and this may enhance scale deposition.
Based on the measured parameters the water can be used for other domestic purposes.
The water is not suitable for irrigation.

General Remarks:

The conclusions and recommendations follows World Health Organization (WHO) guidelines (1994). The conclusions are based only of the parameters measured.
Shallow wells, springs, surface water: *The chemical components of the water is likely to change during a season.*
Deep wells: *The chemical components of the water is likely to change in the first period after drilling the borehole, it is therefore recommended to retest the water after e.g. 6 months.*
Test Methods: *the test methods follows the "Standard Methods for the examination of Water and Wastewater" published by American Public Health Association and American Water Works Association.*
Further information *on the individual test is available in the folder "Interpretation of Water Test Results" from CDN Water Quality.*

CDN Water Quality Laboratory — *12-Nov-09* *Date*

CDN WATER LABORATORY
TEL: 051 - 2216264/5
FAX: 051 - 2214151
12 NOV 2009
Email- cdnwaterlaboratory@yahoo.com
P.O. Box 938, NAKURU, KENYA

* MAJI NI UHAI * WATER IS LIFE *

WATER QUALITY

Catholic Diocese of Nakuru Water Programme

P.O. Box 938
Nakuru
KENYA

Tel.: +254 - 51 - 2216 264/5
Mob: +254 - 0722 867 551

Telefax: + 254 - 51 - 2214 151
E-Mail:cdnwaterquality@yahoo.com

When replying please quote our Ref. No.

Our ref.: *091103NWG T712*

Test type: *Standard Chemical Water Analysis*

Submitted by: *Samuel P.Harrell*

Date received: *06-11-09*

Source: *Filtered*

Date taken: *?*

Physical and Aggregate Properties:	***Results***	***Units***
Temperature		°C
Colour (true)	*15*	Colour units/l
pH	*7.9*	
Turbidity	*2*	NTU
Conductivity	*254*	mS/m
Acidity (pH=8.3)	*30*	mg $CaCO_3$/l
Acidity (pH=10.8)	*1414*	mg CaCO3/l
Alkalinity (phenolpthhalein)	*0*	mg $CaCO_3$/l
Alkalinity total (pH=4.5)	*1354*	mg $CaCO_3$/l
Hardness total	*23*	mg $CaCO_3$/l
Total solids (residue dried at 110C)	*2246*	mg/l
Total dissolved solids (residue dried at 180C)	*1985*	mg/l
Settleable solids	*Less than 0.1*	ml/l
SAR (Sodium Absorption Ratio)	*23.7*	-
RSC (Residual Sodium Carbonate)	*26.7*	meq/l
SI (Saturation index)	*0.6*	
Metals:		
Calcium (Ca^{++})	*7*	mg/l
Iron (Fe^{+++})	*0.3*	mg/l
Magnesium (Mg^{++})	*1*	mg/l
Manganese (Mn^{++})	*Less than 0.1*	mg/l
Sodium (Na^{+})	*520*	mg/l
Inorganic Nonmetallic constituents:		
Carbon dioxide (CO_2)	*31.5*	mg/l
Bicarbonate (HCO_3^-)	*1638*	mg/l
Carbonate (CO_3^{--})	*6.4*	mg/l
Chlorine (Cl)	*Less than 0.05*	mg/l
Nitrate + Nitrite (NO_3^--N)	*1*	mg/l
Total Reactive Phosphorous (P)	*0.2*	mg/l
Chloride (Cl^-)	*46*	mg/l
Fluoride (F^-)	*9.7*	mg/l
Silica (SiO_2)	*31*	mg/l
Sulfate (SO_4^{--})	*256*	mg/l

CDN WATER LABORATORY
TEL: 051 - 2216264/5
FAX: 051 - 2214151
17 NOV 2009
Email: cdnwaterlaboratory@yahoo.com
P.O. Box 938, NAKURU, KENYA